UNIVERSITY OF CALIFORNIA SAN DIEGO

The Utilization of NHS-Biotin Labeling Strategy to Investigate Long Range Axonal Protein Transport in the Developing Rodent Brain

A Thesis submitted in partial satisfaction of the requirements for the degree Master of Science

in

Biology

by

Erika Barth

Committee in charge:

Professor Hollis T. Cline, Chair
Professor James Kadonaga, Co-Chair
Professor Yimin Zou

2020

The thesis of Erika Barth is approved, and it is acceptable in quality and form for publication on microfilm and electronically:

_____

_____

Co-Chair

_____

Chair

University of California San Diego

2020

TABLE OF CONTENTS

LIST OF FIGURES

LIST OF TABLES

LIST OF GRAPHS:

ACKNOWLEDGEMENTS

I would like to acknowledge Lucio Schiapparelli for being my mentor in the lab and teaching me all the techniques that I have applied to my thesis. From immunohistochemistry to biochemistry and animal handling, Lucio taught me all of the skills that I have acquired during this Master's program. I am very grateful for his patience and willingness to teach.

I would also like to acknowledge the additional work done by other members of the Cline lab, in particular Ana Araujo, our lab tech. Ana helped significantly with conducting the western blots to validate our injections and homogenize all the samples. She also helped with precipitating our mass spectrometry samples. The immense volume of samples would have been unmanageable without her assistance. I would also like to thank Pranav Sharma, for teaching me some advanced tips about confocal imaging. The image quality significantly improved with your help as well as your contribution of the image in figure 7A. Thank you to Victoria Nudell for performing the CLARITY protocol to provide us with whole-brain images in figure 4. I would also like to acknowledge every other member of the Cline Lab that gave me feedback during lab meeting presentations and were a guiding force in my learning.

Lastly, I would like to acknowledge my thesis advisor, Holly Cline. I appreciate the opportunity you gave me to work in your lab. You have been an outstanding mentor. Thank you to the rest of my thesis committee, in addition.

ABSTRACT OF THE THESIS

The Utilization of NHS-Biotin Labeling Strategy to Investigate Long Range Axonal Protein Transport in the Developing Rodent Brain

by

Erika Barth

Master of Science in Biology

University of California San Diego, 2020

Professor Hollis T. Cline, Chair
Professor James Kadonaga, Co-Chair

The Cline Lab has used N-hydroxysuccinimidobiotin (NHS-Biotin) in proteomic analysis of the visual system by labeling neuronal projections from the eye to the Superior Colliculus (SC) and the Lateral Geniculate Nucleus (LGN), in adult rats *in vivo*. Using intravitreal injections, NHS-Biotin labels endogenous proteins in the retina that are then transported to various retinal targets in the visual system. NHS-Biotin protein labeling allows the identification and investigation of the population of proteins transported in long-range axonal projections. The covalently bound biotin is used as a tool for immunoprecipitation to conduct biochemical and proteomic analyses. Here, we are interested in adapting the NHS-Biotin protein labeling technique to allow precise study of transportomes in the developing mammalian nervous system *in vivo.* We tested whether NHS-Biotin can be used to study projections in the developing brain, tracing connectivity, as well analyzing the proteomic composition by mass spectrometry. We addressed these questions in the following experiments by conducting unilateral intracortical

injections of NHS-Biotin into post-natal day 3 rat pups. We used western blots to compare the levels biotinylated protein in the injected (ipsilateral) and contralateral cortical hemispheres. We probed NeutrAvidin enriched biotinylated endogenous proteins for known axonal proteins, such as MAPK, Tau, and β-synuclein, and found that they showed significant intercortical transport via the corpus callosum, anterior commissure and cortical-spinal tract. These data demonstrated that NHS-Biotin can be used in the morphological and biochemical study of long-range axonal projections in the developing rodent brain following targeted injections. To test whether we could use the NHS-Biotin labeling strategy for mass spectrometric proteomic analysis of the developing cortical transportome, we used the Direct Detection of Biotin-containing Tags (DiDBiT), which increases the sensitivity of biotinylated protein detection. The mass spectrometry data show the proteomic landscape of the axonally transported proteins across the corpus callosum. This paper reviews previous labeling strategies and limitations of these techniques, while introducing a novel strategy that overcomes many of these limitations. The experiments we conducted highlight how the NHS-Biotin labeling strategy allows efficient identification and investigation of axonally transported proteins.

Introduction:

The interconnectivity of the brain is innately complex and the most convoluted yet highly organized structure of the human body. All physiological functions ranging from movement to memory and emotions are coordinated by the brain, yet only weighs around 2% of the total human body. How does this incredible system mediate all tasks and cognition? We know that on average each person has upwards of 80 billion neurons with over hundreds of trillions of synaptic connections. This intangible level of organization and connectivity has inspired computer networks and artificial learning code; however, nothing close to the extent of the human brain has been conceived. All functions of the brain from development to synaptic plasticity and synaptic transmission are mediated at the interface of protein-DNA interactions. Primarily protein interactions and transport in the brain are the crux of investigating the interconnectivity of neural networks. Due to the crude fact that structure determines function, the tracing of cytoarchitecture has been at the forefront of neuroscience for hundreds of years.

The field of neuroscience has made exponential leaps since the introduction of neuronal circuit tracing strategies. The significance of this paper is to review the development of these strategies as well as introduce a new endogenous protein labeling technique that overcomes many limitations posed by these previous strategies. From the introduction of Golgi Staining to use of viruses that express fluorescent proteins, molecular biologist and neuroscientists have developed molecular tools to understand the complex and interconnected network of the nervous system, in particular, the intricate circuitry of the brain. By reviewing previous strategies, we can understand their biochemical limitations and better develop new mechanisms to label circuits and investigate the transcriptomes and endogenous proteomic landscape. The Cline Lab developed the N-hydroxysuccinimidobiotin (NHS-Biotin) labeling strategy, initially used in the visual

system; however, this paper will highlight experiments that demonstrates its versatile applicability to long-range axonal projections throughout cortical and subcortical regions in the developing rodent brain. NHS-Biotin was previously used to trace retinal ganglion cell projections to the lateral geniculate nucleus (LGN) and the superior colliculus (SC) to investigate the population of transported proteins through the optic nerve. With astounding results from these experiments in the visual system, the question was raised whether this strategy could be applied to investigate long-range projections throughout the developing central nervous system. To answer this primary question, we used NHS-Biotin to trace cortical projections across commissures and to the spinal cord, by conducting unilateral intracortical injections into rat and mouse pups. Using immunohistochemical processing, we visualized the intercortical and subcortical projections both at meso and microscales, to broadly identify these dynamic pathways and closely investigate the localization of biotinylated proteins to axonal projections. Beyond the tracing applications, we conducted biochemical analysis to identify and investigate the transportome of these intercortical and subcortical projections. Using both biochemistry and the previously developed DiDBiT (direct detection of biotin containing tags) method for mass spectrometry, the proteins transported through long range projections in the developing rodent brain are well described in the results of these experiments. Using a microdissection strategy to isolate the corpus callosum and cortical tissue from the ipsilateral and contralateral hemispheres, we conducted western blots to investigate axonal candidates to detect individual proteins labeled and transported along these projections. Some of these candidates include Tau, MAP2, mTOR, synapsin, CAMKII, BDNF, NF-m and β-synuclein, which allowed us to investigate cytoskeletal proteins, synaptic proteins and transcription factors. We utilized the DiDBiT method of protein digestion and peptide enrichment with Neutravidin beads to isolate biotinylated proteins to then

allow for identification and quantification of the population of transported proteins with mass spectrometry. These results showed significant enrichment of cytoskeletal proteins and axon guidance molecules transported from the ipsilateral cortical injection site, through the corpus callosum to the contralateral cortex. As expected all proteins identified in the corpus callosum were also present in the contralateral cortex, as the corpus callosum simply poses as a biochemical highway between the two hemispheres. Our mass spectrometry proteomic data demonstrated significant biotinylation of guidance molecules such as Nrcam and proteoglycans, involved in Ephrin mediated signaling pathways, consistent with the developmental stage of the rat pups. Using the NHS-Biotin labeling strategy not only can we investigate the transportome of long-range axonal projections in rodents during this developmental stage but we can apply this versatile technique to a wide range of studies. Now that this technique has been validated for the use in interhemispheric and subcortical projections, we can repeat these experiments in a range of developmental time points to establish a temporal description of cell adhesion molecules and guidance cues. We can also evaluate the differential transport of this subpopulation of proteins in rodent models of human neurological diseases. We can also repeat these experiments in a range of developmental time points to establish a temporal description of cell adhesion molecules and guidance cues. Furthermore, with the numerous neurodevelopmental diseases that are associated with abnormal commissure formation we may be able to shed light on proteomic disruptions causing these misprojetions and aberrant axon guidance.

Chapter 1: Circuit Tracing and Protein Labeling Strategies

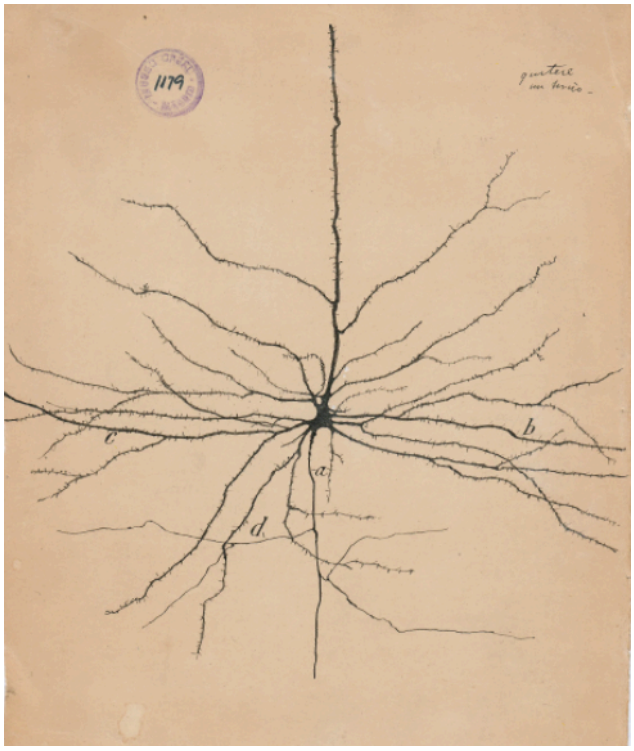

Figure 1. Ramón y Cajal. Pyramidal Neuron of the Cerebral Cortex, 1904. Credit: Cajal Instiute (CSIC),

With the complexity of the nervous system, circuit tracing provided an insight into the interconnectivity of the brain and the peripheral nervous system. The foundation of neuroanatomy was initiated by tracing the connectivity of neural circuitry. Santiago Ramón y Cajal, the father of neuroscience, contributed the first accurate representations of neurons by using silver-based golgi staining. Of course, high resolution imaging had not been established at this time, so the artistic talent of Ramón y Cajal played a major role in profiling these tracings. Prior to the use of Golgi staining, Wallerian Degeneration was used to determine connectivity by creating lesions in the brain. However, with the development of the Golgi stain, a neuroanatomical revolution began. There were many limitations with this first staining technique, as it did not allow for the visualization of long-range projections, narrowing the

application to single neuron tracing, without clear information on the distribution of axons or neuronal connections in circuits.

As the first labeling strategy was developed, Bernice Grafstein and Paul Weiss established a radiolabeling strategy using tritiated amino acids (Saleeb et al, 2019). This technique employed endogenous protein transport as a mechanism to trace the axons from the soma to its terminal. This was the first method of anterograde labeling, leading to significant findings in long range axonal projections, especially in the visual system. The use of radiolabeled leucine established a platform for an unlimited amount of experiments that could be conducted to investigate the transport of endogenous proteins within the nervous system. With this technique, there were major advances in cytoarchitecture and the rate of protein transport throughout the central and peripheral nervous system. However, a more refined technique was necessary to both validate these findings and launch a new wave of discoveries.

The introduction of Horseradish Peroxidase (HRP) was critical and propelled all fields of biological sciences. The first documented use of HRP was in 1971, when it was conjugated to albumin and injected intramuscularly into a rat (Kristensson and Olsson, 1971). Labeled spinal motor neurons were visualized due to the uptake and transport of the conjugated albumin. HRP was a major leap in neuroanatomical advances due to the versatility of the technique and the ability to visualize the label with light and electron microscopy. HRP is still used in modern day assays due to its wide range in applications, from biochemical to histochemical analysis. However, due to endogenous peroxidases in compartments of the cell body, there was significant background signal that overshadowed the primary signal. Furthermore, the colorimetric assay lacked sensitivity, which convoluted and limited many findings. Due to these limitations, scientists developed new strategies and the era of neurotropic viruses began.

Cholera Toxin-B (CTB) allowed for rapid and non-pathogenic retrograde labeling of neurons. The conjugation of HRP to CTB was a major turning point for circuit tracing because it conceived of viral vectors as both tracing strategies as well as delivery mechanism for markers, transgenes, and therapeutics. The sensitivity of CTB-HRP increased 60 fold compared to native HRP, by the use of immunhistochemical processing (Saleeb et al, 2019). Furthermore, neurons took up HRP via passive endocytosis, whereas CTB-HRP was taken up by receptor mediated endocytosis, providing more reliable and replicable delivery (Wouterlood et al, 2020). With the conjugation of HRP to CTB, there was a prolonged life of signal whereas the native HRP would have been degraded *in vivo.* Lastly, the speed of transport was significantly faster with the conjugated virus than the native HRP.

With these improvements to HRP tracing, the field turned to neurotropic viruses as a tracing mechanism when research was conducted on Herpes Simplex Virus (HSV). Using previous data about the viruses, it was known to infect axon terminals and transport retrogradely towards the central nervous system. The major advantage in the initial discovery of viruses as tracers was the innate amplification from the natural replication of the virus. The transsynaptic labeling was a new tool to visualize whole neural networks, rather than one neuronal projection. Previously detected by antibodies, binding to nucleoproteins produced by the virus, visualization was poor and fine structures such as axonal projections and dendritic spines could not be resolved. With the major advances made in virology and molecular biology, recombinant viruses became the most advantageous tracer in neuroscience. Nancy Chamberlin used a recombinant adeno-associated virus as a vector to deliver GFP. Using microinjections, she visualized long distance anterograde transport of the virus by confocal microscopy (Chamberlin et al, 1998). This paper was a turning point in the repertoire of techniques available to neuroscientists.

Recombinant viruses became the newest mode of visualizing neural circuitry. With the additional component of LacZ or Cre dependent expression, the technique became even more selective in its labeling. With Cre-Lox transgenic mice, the viral GFP cassette expression was localized to specific subpopulations, with high spatial and temporal control.

As molecular biology tools developed, the delivery of transgenes and heterogenous nucleotide molecules were injected and electroporated into brains of a wide variety of species to both replicate disease models, deliver therapeutics and visualize circuits. The main limitation that was shared by these tracing strategies was that it lacked versatility for these labeling mechanisms to be applied to biochemical and mass spectrometry analysis. Immunohistochemical analysis is only one part of the neuroanatomical puzzle and is expensive and time consuming to identify all proteomic candidates of the total population. Therefore, the Cline lab developed the NHS-Biotin labeling strategy to address these concerns. This new strategy allows for the identification and analyzation of subpopulations of proteins by biochemical assays and mass spectrometry.

Chapter 2: Development of NHS-Biotin Labeling Strategy

2.1 Background

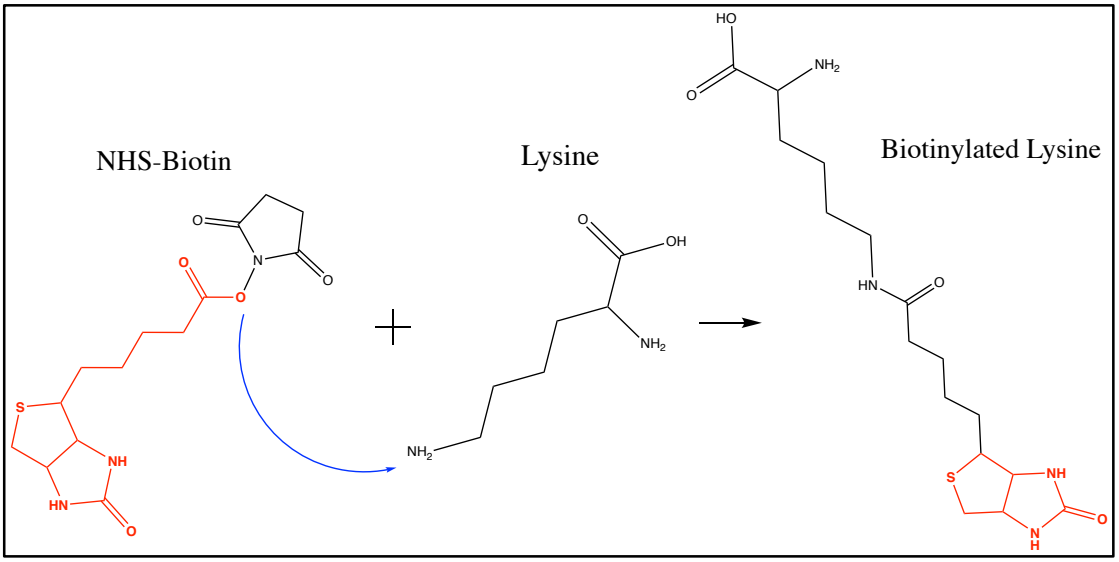

Figure. 2 The conjugation of NHS-Biotin to Lysine amino acid residues

Biotin is commonly used in biochemistry and immunohistochemistry studies due to the availability of many substrates that bind to biotin. Avadin is the most common substrate to immunoprecipitate biotinylated proteins and label *in vivo* for visualization. NHS-Biotin by nucleophilic attack binds to the primary amine of lysine residues to create this single use labeling strategy. Once conjugated, this amino acid label is stable *in vivo* and can be used in immunohistochemical processing. Furthermore, if these proteins undergo lysosomal or proteosomal degradation, the Biotin cannot be reincorporated into other proteins. This inability for biotin to be reincorporated decreases the probability of off-target labeling, especially during the investigation of long-range projections. Biotin is commonly used in biological research, ranging from the use of Biotinylated Dextran Amines (BDA) to biotin derivatives such as Biocytin to Neurobiotin. The major difference between NHS-Biotin is that it is conjugated to individual endogenous proteins unlike the previous strategies which allows for co-histological evaluation and immunoprecipitation for biochemical and mass spectrometry analysis.

2.2 Previous Applications of NHS-Biotin Labeling Strategy

The Cline Lab used NHS-Biotin in previous *in vivo* studies in the visual system. NHS-Biotin was injected intravitreally to label the retinal ganglion cell transportome. Using this labeling strategy, they identified the proteomic populations that were transported along the optic nerve to the two major projections of the visual system; the lateral geniculate nucleus (LGN) and the superior colliculus (SC). They found approximately 350 retinal proteins that were differentially transported to the LGN and SC via the optic nerve (Schiapparelli et al, 2019). This project utilized three modes of analysis; immunohistochemistry, biochemistry and mass spectrometry identification of biotinylated proteins. Further, they used electron microscopy to

localize the endogenous biotinylated transported proteins to the presynaptic compartments in the LGN and SC. This newly developed labeling strategy improved resolution of endogenous protein identification. Further, it allowed for investigation of differential protein transport in optic crush experiments. One major question raised from this paper, was whether this technique could be applied to analyze fiber pathways by conducting cortical injections.

2.3 DiDBiT Mass Spectrometry

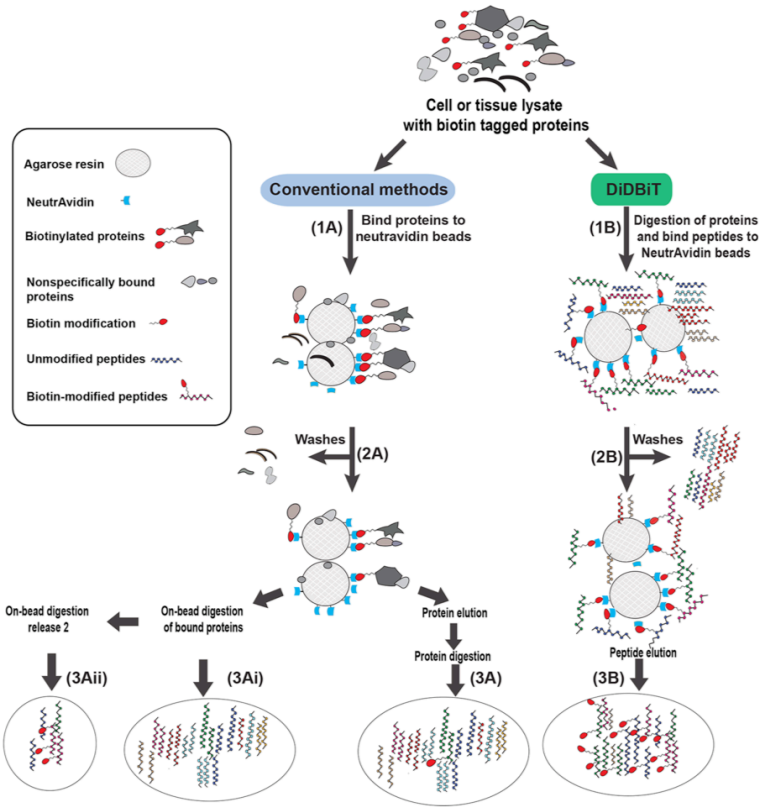

Figure. 3 Variation in protocol from conventional methods (1A) and DiDBiT (1B), yielding more sensitive peptide enrichment (3B). Image credit: (Schiapparelli et al, 2014)

To increase sensitivity of mass spectrometry, the Cline Lab developed a method to directly read biotinylated proteins, called Direct Detection of Biotin-containing Tags (DiDBiT). Previous techniques using a biotin tag are less sensitive and does not allow for accurate discrimination between biotinylated proteins and untagged contaminants. Previous methods

enriched samples by binding the proteins to avidin conjugated to beads, followed by elution and digestion or digestion on the beads and elution. However, the major differentiating factor that increases the sensitivity of DiDBiT 200 fold, is that the proteins are digested prior to enrichment (Schiapparelli et al, 2014). By conducting the digestion step prior to enrichment, interactions between untagged proteins and biotinylated proteins as well as interactions between untagged proteins and the beads are significantly reduced. Minimal contamination allows for higher resolution analysis of the labeled endogenous proteins, as contamination disrupts the accurate representation of the transportome.

Chapter 3: New Applications of the NHS-Biotin Labeling Strategy

The major question regarding the NHS-Biotin labeling strategy was whether it could be applied to cortical and subcortical axonal projections, as it has only been used in the visual system to investigate the transportome of retinal ganglion cells to the LGN and SC. We conducted experiments to answer this question by injecting NHS-Biotin intercortically into the left hemisphere of rat pups.

3.1 Administration of NHS-Biotin - Unilateral Intercortical Injection Strategy

We conducted these experiments in post-natal day 3 rodents due to the delayed development of the skull; we therefore injected unilaterally with a micropipette through the epidermis and dura of the pup without prolonged surgery. We used DMSO as a vehicle and Fast Green to spatially localize the injection to approximately 2 mm caudal and 3 mm medial of the eye. Each pup was injected with 4 μL of the vehicle containing the dye and NHS-Biotin. The validation of the injection strategy will be discussed during the analysis of the biochemistry studies.

3.2 Investigation of Cortico-Spinal Tract Protein Transport

To visualize the entirety of the spinal cortical projection, CLARITY was used due to the benefit of whole brain imaging. Following the intercortical injections at p3 in rats, the pups were sacrificed at p8 by transcardial perfusion with 4% PFA, followed by a post-fix in 4% PFA for 24 hours. This approach was used to outline the connectome at a mesoscale level to better prepare us for microscale investigation with immunohistochemistry.

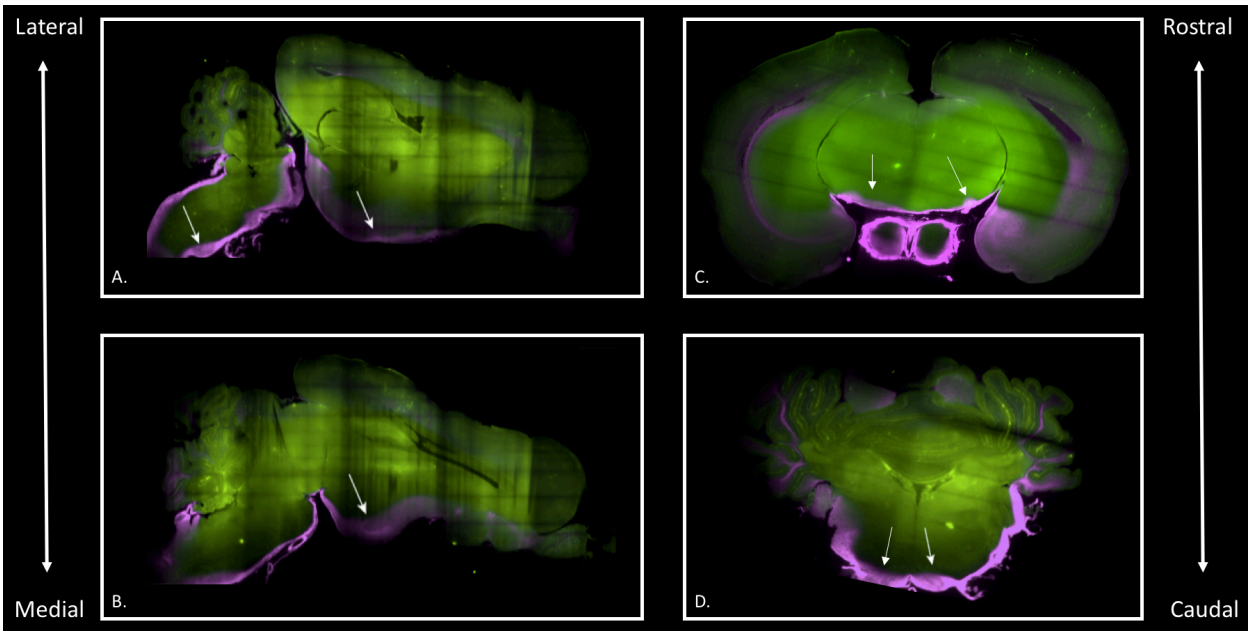

Figure. 4 Immunostained whole brains of p8 rat using streptavidin to visualize endogenous biotinylated protein, in purple. ROI: cortico-spinal tract. **A.** Lateral position of sagittal view. **B.** Medial position of sagittal view. **C.** Hindbrain position of coronal view. **D.** Cerebellum in coronal view. (Credit: Nudell, 2019)

In **figure 4**, the purple is the streptavidin label, showing the cortico-spinal projection from our initial unilateral cortical injection with NHS-Biotin. Using the Allen Brain Atlas as a reference for localizing the cortical spinal tract (CST), we deduced that this labeling projected subcortically from the ipsilateral cortex to the internal capsule and cerebral peduncle, forming the pyramidal tract through the hindbrain and into the spinal cord. Both **figure 4. A** and **4. B** show the CST through the cerebral peduncle, via a sagittal view, laterally and medially, respectively. In **figure 4. C**, we visualized the pyramidal tract in the hindbrain projecting from

the cortex to the spinal cord. Lastly, **figure 4. D** traced the CST through the most ventral area of the cerebellum, indicated by the arrows. The whole brain imaging provided by the CLARITY protocol allowed for more precise sectioning and immunohistochemical processing to evaluate the CST.

To investigate the CST on a microscale, we used immunohistochemistry to visualize the biotinylated endogenous protein signal by anti-biotin antibodies. The investigation was initiated by repeating intercortical injections and perfusing intracardially at p8. In **figure 5. A**, a whole brain coronal section was used to visualize the mesoscale of biotinylated endogenous protein transport in the developing rodent. The regions of interest in this whole brain image are highlighted in white boxes to show the intercortical projections and the cortico-spinal projections, respectively. In **figure 5. B**, from a 40X magnification we visualized individual axonal projections with biotinylated protein cargo that was transported over the five-day period to the contralateral cortex, caudal of the injection site. In **figure 5. C**, we also see individual

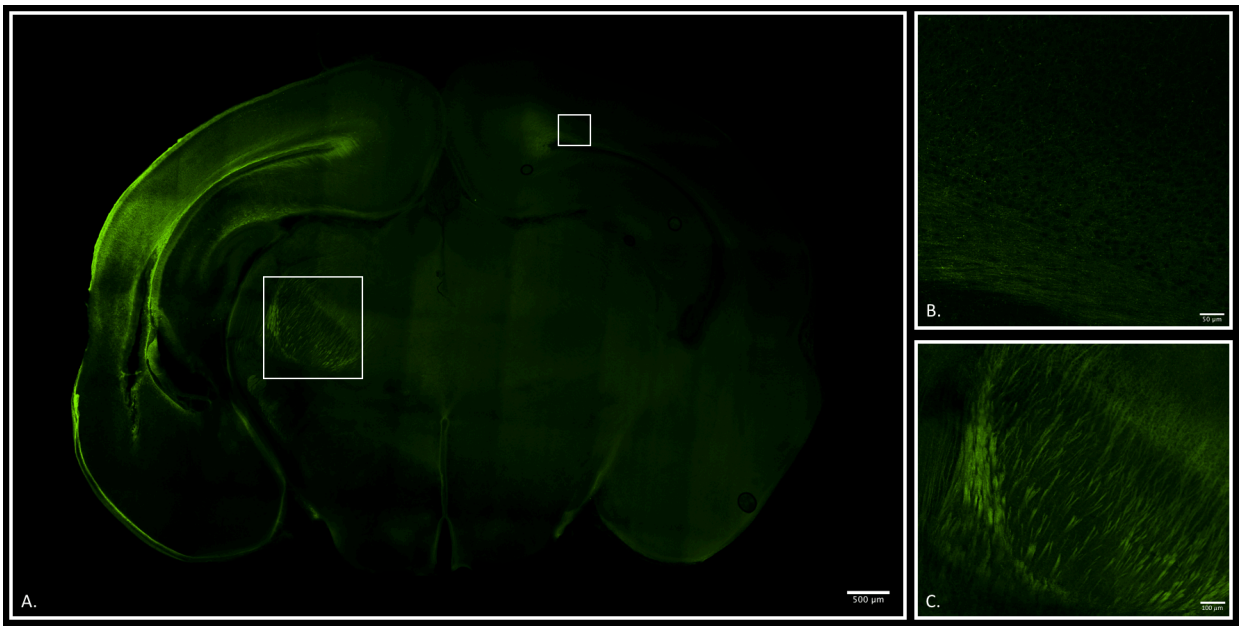

Figure. 5 Immunostained coronal sections of p8 rat with anti-biotin in green, (50 μm) sections. **A.** Whole brain, coronal section. ROI: a. contralateral cortical projections to hindbrain. b. cortico-spinal tract via striatum. **B.** Contralateral cortex, 40X magnification. **C.** Striatium, indication of cortico-spinal projection.

axonal projections and endogenous biotinylated cargo transported along the CST through the internal capsule towards the cerebral peduncle.

After analyzing these immunohistochemical images, we sectioned more caudal areas of the developing rat brain to investigate the brainstem and the final projection into the spinal cord. We found that the last detectable signal of biotinylated protein was found in the brainstem. Potentially due to either low signal to noise ratio or lack of sufficient time for protein transport, we were unable to visualize significant biotinylated signal in the spinal cord. In **figure 6. A**, the coronal section of the brainstem showed prominent biotinylated proteins in the most ventral area,

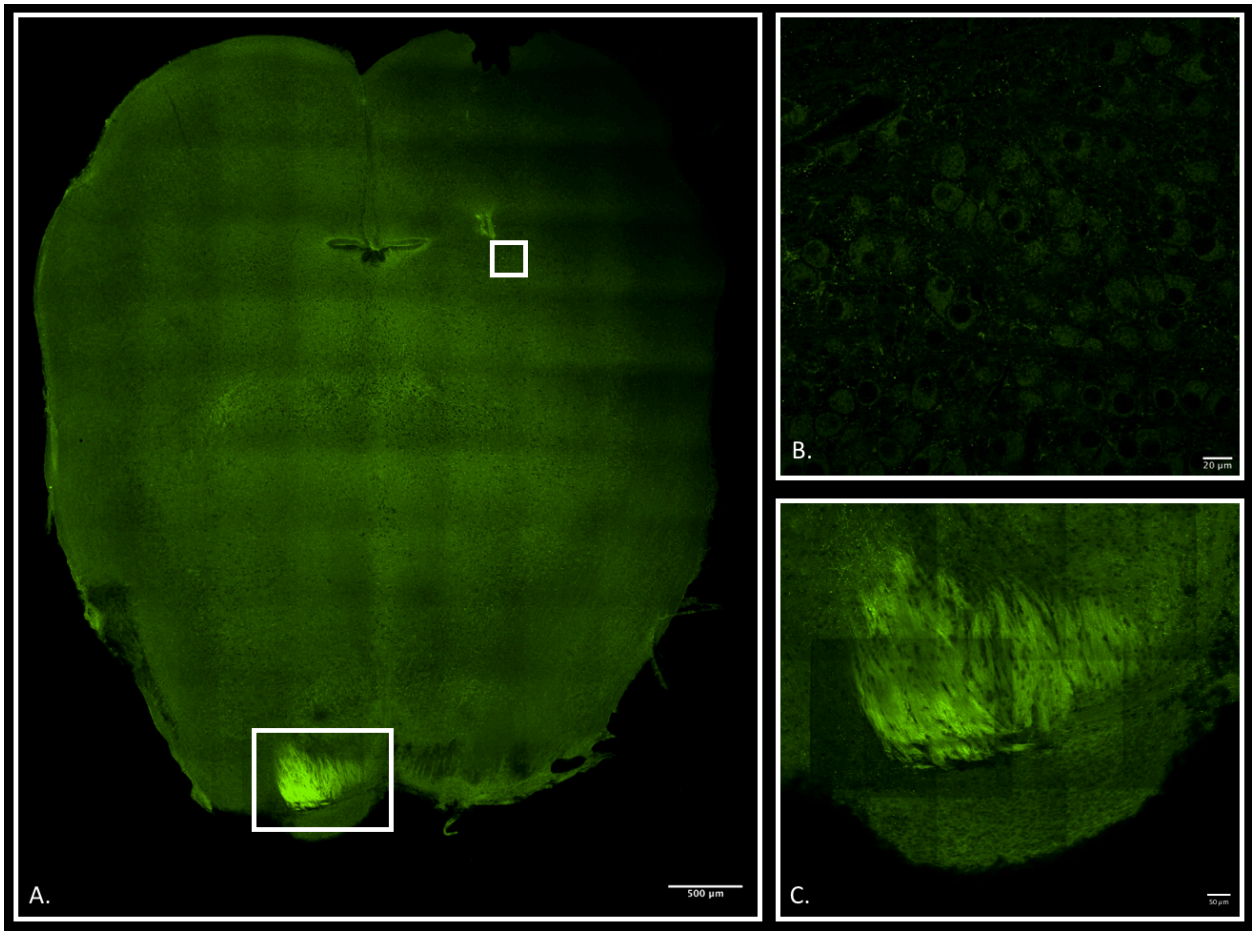

Figure. 6 Immunostained coronal sections of p8 rat with anti-biotin in green, (50 μm) sections. **A.** Whole brain, coronal section. ROI: b. Hindbrain biotinylated endogenous protein signal. b. Cortico-spinal tract in hindbrain. **B.** 40X magnification. **C.** Cortico-spinal projection, identified by referencing Allen Brain Atlas coronal mouse sections.

where previous studies has localized the cortico-spinal tract to. The region of interest is highlighted by the larger white box to show the significant biotinylated protein transport along this long-range projection. **Figure 6. C**, shows a magnified image of this axonal pathway and the enrichment of biotinylated proteins transported, initially labeled in the ipsilateral cortex. The cortico-spinal tract crosses the brain, so the enriched signal is present in the contralateral hemisphere to the injection site, as predicted. **Figure 6. B**, is used to represent the background signal of biotin. This signal is localized to cell bodies, which further indicates the labeling of endogenous carboxylases.

3.3 Investigation of Intercortical Protein Transport

3.3.1 Histological Evaluation

Using immunohistochemistry, we visualized endogenous biotinylated protein via anti-biotin antibodies. After the injection of NHS-Biotin, the conjugation of biotin to the lysine of

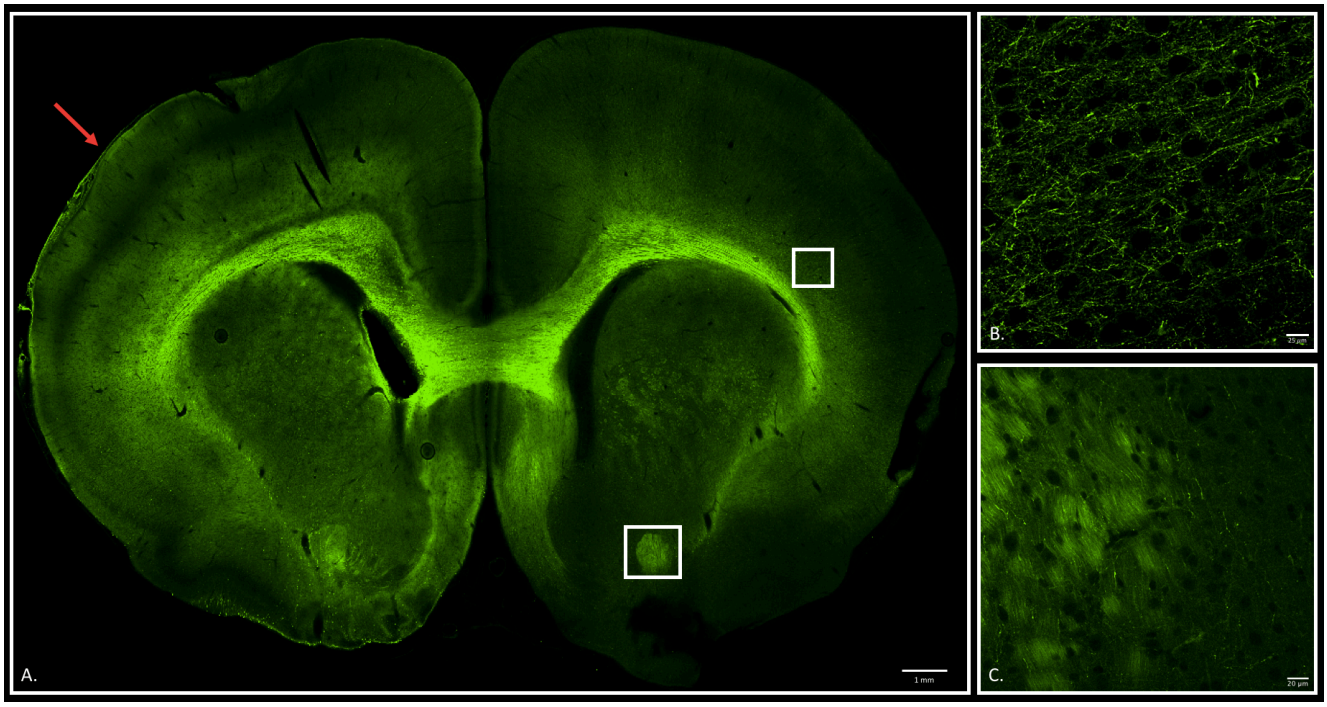

Figure. 7 Immunostained coronal sections of p8 rat with anti-biotin in green, (50 μm) sections. **A.** Whole brain, coronal section. ROI: b. Contralateral cortex. c. Anterior commissure. **B.** 60X magnification of contralateral corpus callosum. **C.** 40X magnification of anterior commissure, identified by referencing Allen Brain Atlas mouse coronal sections. (Credit: Sharma, 2019).

proteins allows for the definite and irreversible labeling of these endogenous proteins. Using both whole brain imaging techniques and 50 μm immunohistochemical sections, we visualized both local and long-range transport of these biotinylated proteins. We found that prominent signal was localized to commissure fiber pathways such as the corpus callosum and the anterior commissure. As seen in **figure 7. A**, the injection site, labeled by the red arrow, shows labeling of the endogenous biotinylated proteins from the ipsilateral cortex, across the commissure fiber pathways to the contralateral cortex. Many higher magnification images were taken and analyzed to investigate the single axonal transport that occurs. In the 40 and 60x images in **figure 7. B** and **7. C** we can see discrete labeled cargo within the axonal projections in the contralateral cortex. This labeling of cargo being transported along the length of axonal projections is apparent in **figure 8. B**, and **8. C**. The 40x image (**8.C**) of the ventral end of the corpus callosum, shows axonal projections out of the corpus callosum into the contralateral cortex. In **figure 7. A** and **7.**

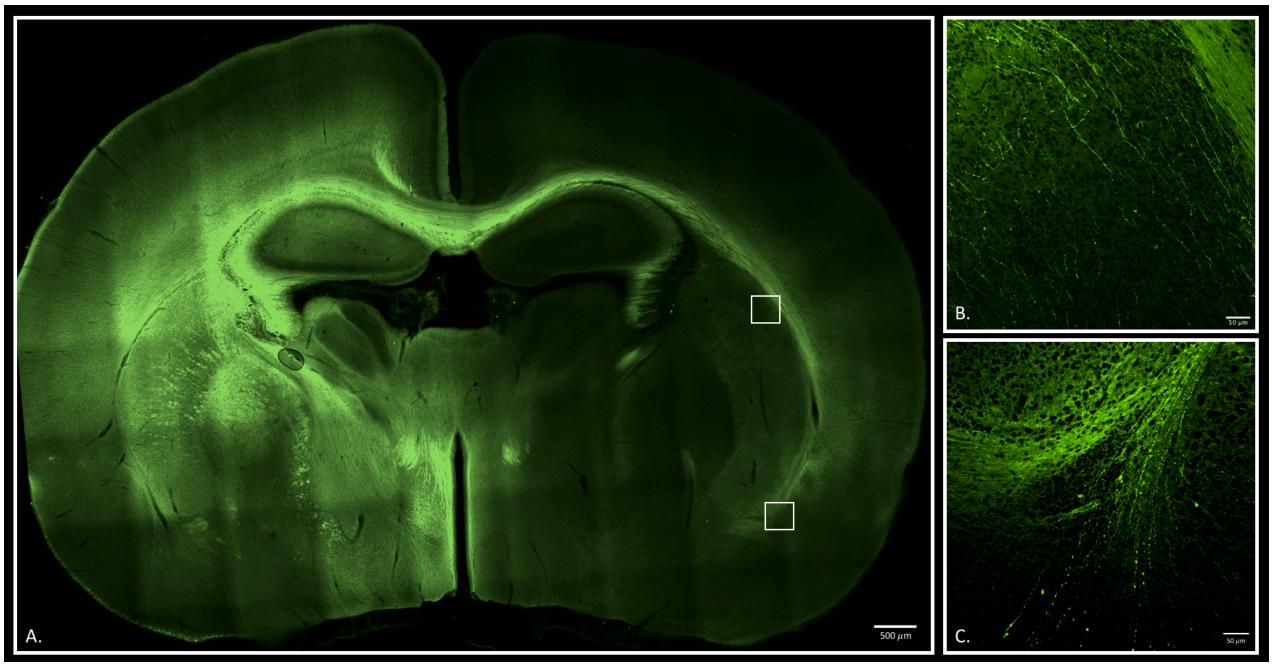

Figure. 8 Immunostained coronal sections of p8 rat with anti-biotin in green, (50 μm) sections. **A.** Whole brain, coronal section. ROI: b. Contralateral corpus callosum with subcortical projections. c. Ventral portion of contralateral corpus callosum with cortical projections. **B.** 40X magnification of contralateral corpus callosum. **C.** 40X magnification of contralateral corpus callosum.

C, we can see the projection of the anterior commissure caudally to connect the two hemispheres; the labeling of this pathway indicates fast axonal transport of proteins from one cortical section to the other hemisphere.

Figure 8. A, a more caudal coronal section than visualized in **figure 7. A**, we determined the significant labeling of the cortical-spinal tract, via the internal capsule labeling on the ipsilateral side as well as the corpus callosum by the distinct contralateral projection. **Figure 8. B** and **C** are magnified images of projections protruding from the corpus callosum into the cortical layers. In **figure 8. C**, especially, we can examine the discrete endogenous biotinylated proteins

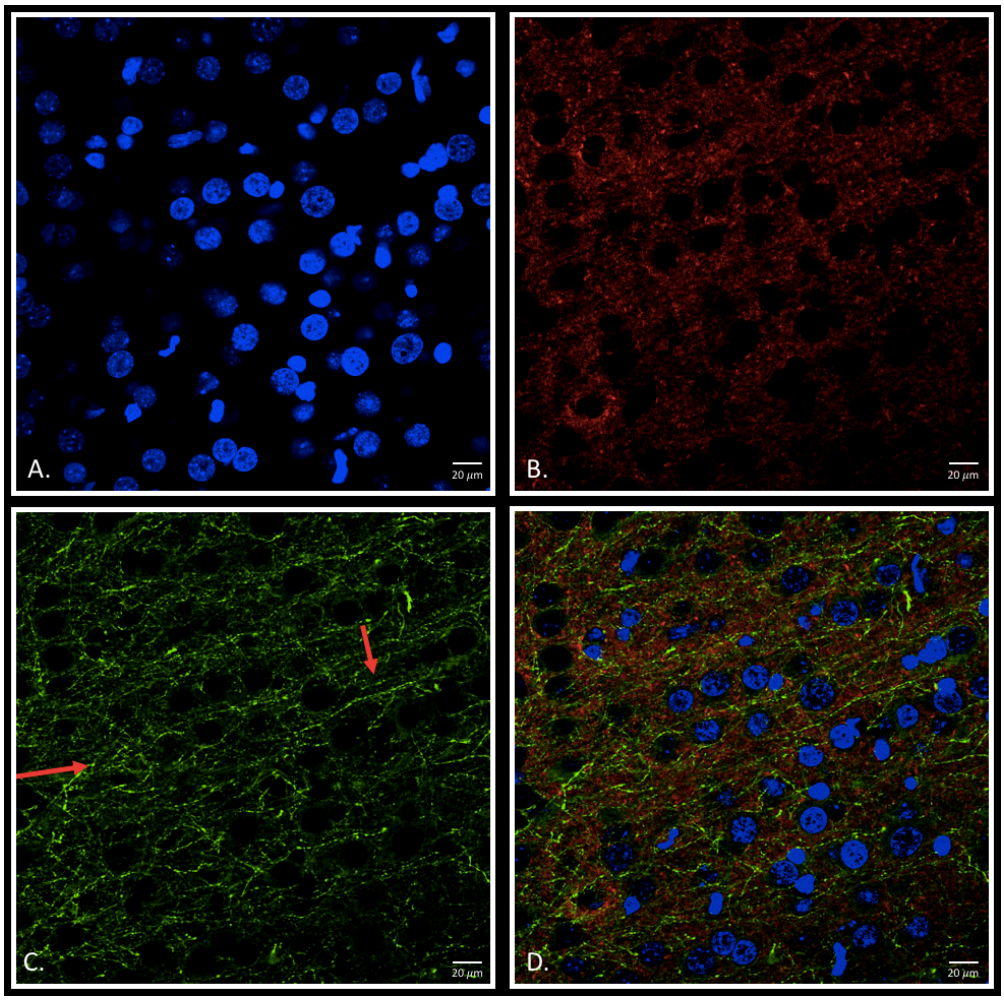

Figure. 9 Immunostained coronal sections of contralateral cortex in p8. **A.** DAPI **B.** Synapsin **C.** Biotin **D.** Merge

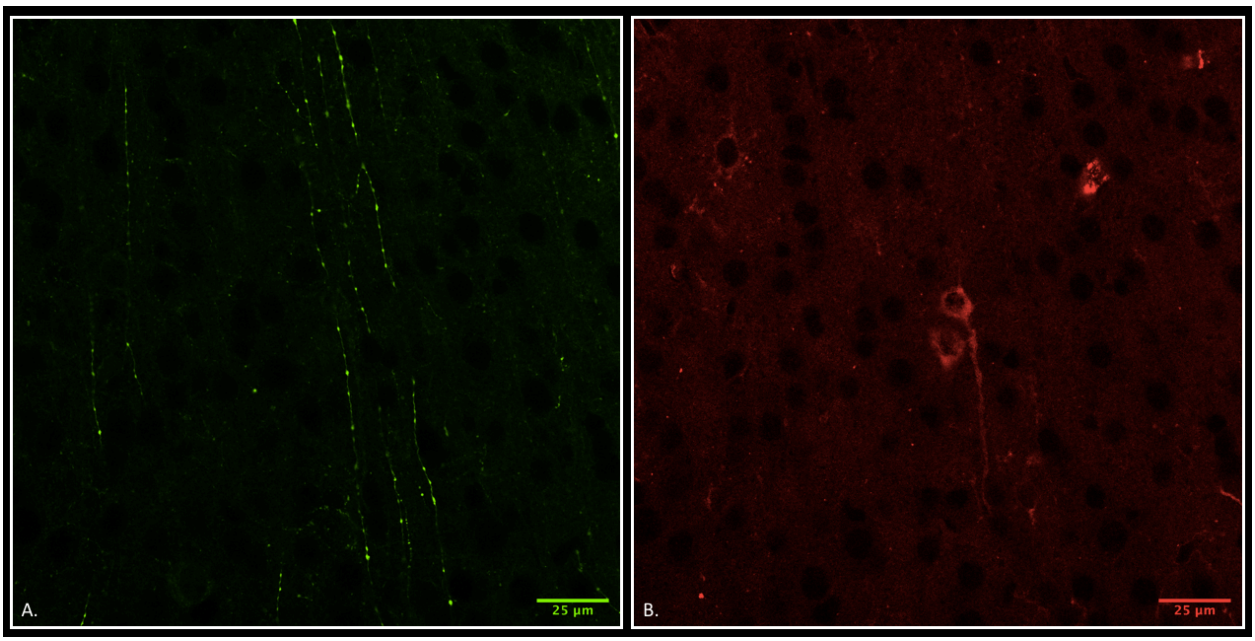

Figure. 10 Immunostained coronal sections of contralateral cortex. 60X image of **A)** Biotinylated Endogenous Proteins **B)** Tau immunostain.

transported through axons by the localized cargo signals. These observations are what lead us to examine, biochemically, both the axonal proteins as well as the synaptic proteins that were presumed to be transported to nascent synapses during this developing time point in the rodent. These proteins visualized are all endogenously labeled proteins and cannot be identified through immunohistochemical techniques and must be investigated using Mass Spectrometry. Using a z stack of images, we colocalized axonal proteins such as Tau, MAP2 and mTOR through orthogonal views. The colocalization of this signal is indicative of these axonal proteins labeled by biotin and the anterograde transport to synapses. This conclusion is supported further by biochemical studies conducted to immunoprecipitate all biotinylated proteins and immunostain for these axonal candidates in western blots.

We used 60X magnified confocal images (**figure 10**) to visualize the colocalization of the biotinylated endogenous protein with axonal candidate Tau. In **figure 10. A** you can visualize the protein cargo within the axonal projections from dorsal to ventral in the contralateral cortex. This

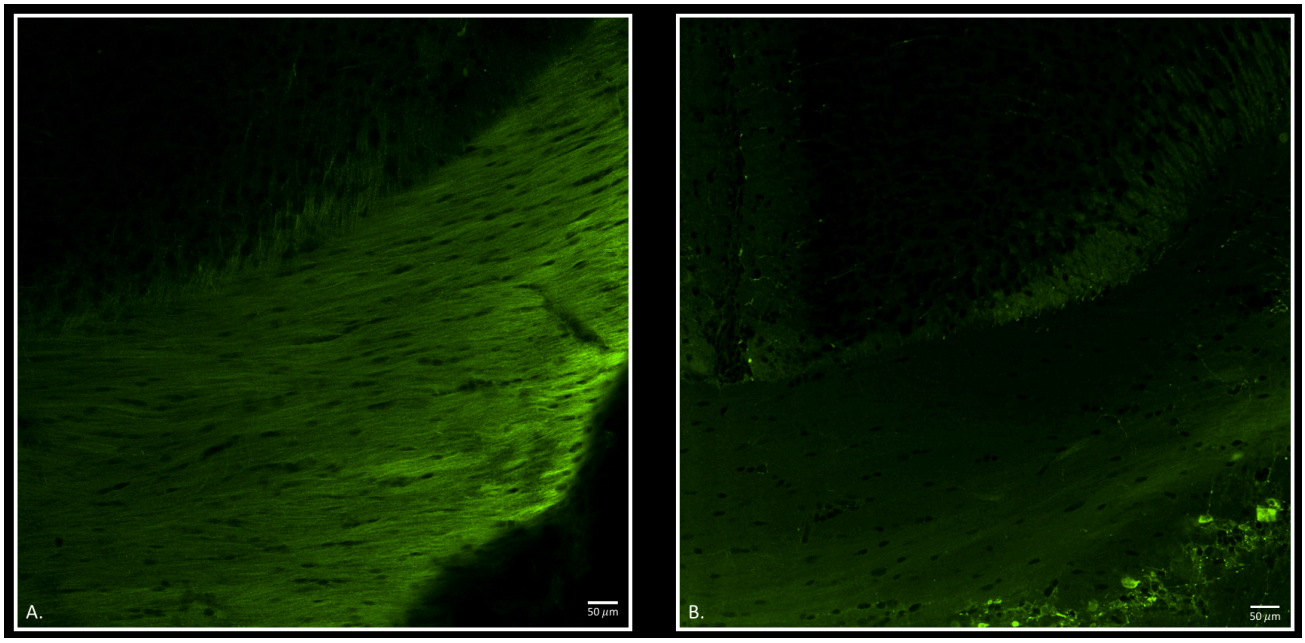

Figure. 11 Immunostained coronal sections of corpus callosum in p8 (**A)** and p4 (**B**) mouse pups.

image is the most ventrolateral cortical region, 2 mm caudal of the injection site. In **figure 10. B** we visualized the staining of Tau along one of these axonal projections.

To further investigate the labeling of endogenous proteins in the developing brain we visualized this signal in a range of different time points. All injections were conducted at postnatal day 3, but we sacrificed the mouse pups on postnatal days 4, 5, 8 and 10. This allowed us to investigate the varying speed of transport across callosal fibers and along the cortical-spinal tract. In **figure 11** we specifically imaged the corpus callosum to evaluate the differential level of biotinylation that had been transported from the ipsilateral cortex. **Figure 11. A** is a p8 mouse pup with extensive corpus callosum labeling and transport of biotinylated proteins, whereas in **figure 11. B**, a p4 mouse pup, we see labeling but the signal was not as pronounced. This could account for the speed of transport of the newly biotinylated proteins from the ipsilateral cortex. There is an increase global signal as the time between sacrificing the animal and the injection date increases but seems to plateau around postnatal day 8.

One limitation to this technique is the background signal that arises from endogenous carboxylases that use biotin as a cofactor. Unlike non-native substances like HRP, biotin exists naturally in rodent brains among other species. However, the signal to noise ratio is significant enough to evaluate the transport of labeled proteins in local neurons and long range projections. This background signal was visualized previously in the evaluation of the cortico-spinal tract in **figure 6. B**.

3.3.2 Biochemical Evaluation

3.3.2.1 Dissection Strategy Validation:

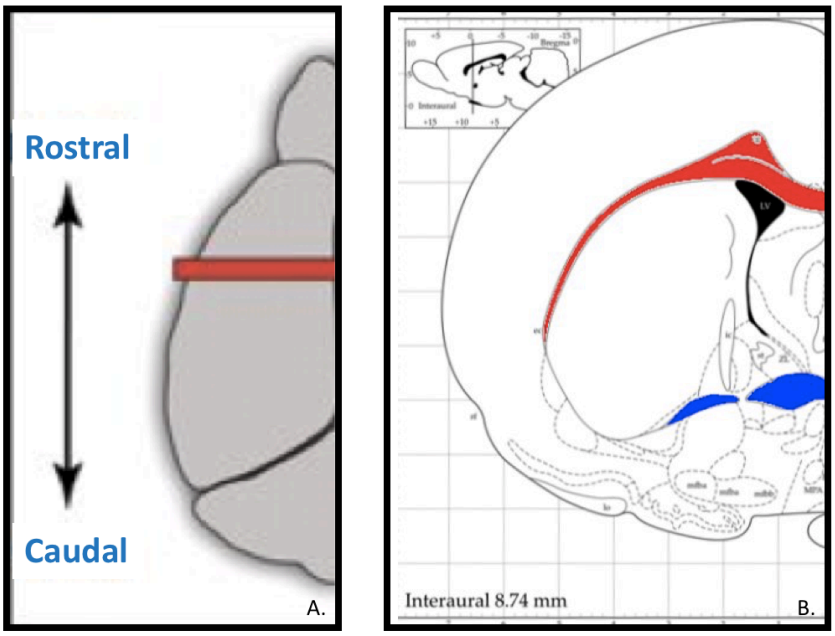

Figure. 12 Dissection Strategy to isolate ipsilateral and contralateral corpus callosum and cortex samples.

To analyze long range axonal projections, we studied the proteomic composition of the corpus callosum as well as cortical areas that project from the injection site through the corpus callosum to the contralateral hemisphere. In order to study these subpopulations extensively, they had to be isolated. We developed a microdissection strategy to isolate four tissue samples with

minimal contamination: ipsilateral cortex, ipsilateral corpus callosum, contralateral corpus callosum and contralateral cortex. To do so we divided the hemispheres of flash frozen rat brains to reduce contamination between the injection site and the contralateral projections. We then made 1-2 millimeter coronal sections to dissect the corpus callosum with as much accuracy using a ten blade, forceps and a dissecting scope. All dissections were conducted over dry ice or in a cold room to maintain tissue viability. The white fiber pathway of the corpus callosum was easily distinguishable from the light pink cortical tissue. After coronal sections were made through the entire brain and the corpus callosum was collected, the cortical tissue from the same sample was collected. These processes were repeated with the ipsilateral hemisphere. Finally, cerebellum samples were collected as a negative control to test for contamination. It was discovered later that due to the cortico-spinal tract labeling there was biotinylation within the contralateral cerebellum tissue.

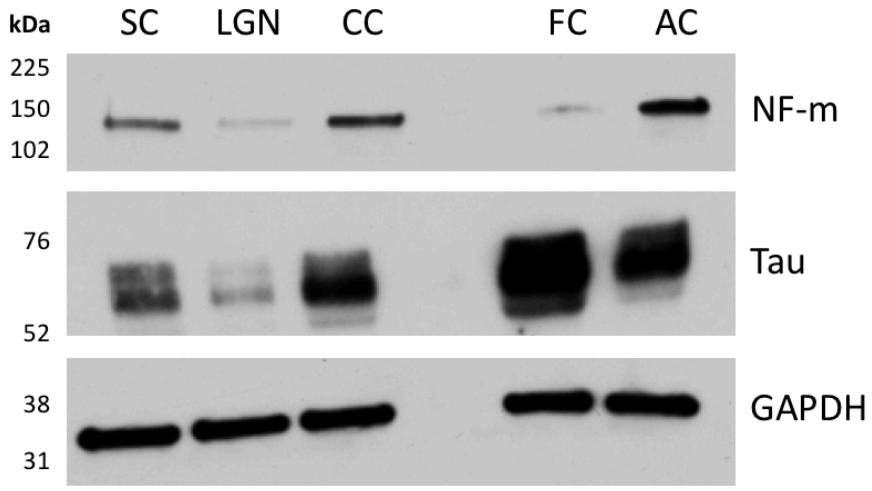

Figure. 13 Western Blot to validate microdissection strategy by analyzing axonal protein enrichment in axonal fiber pathways and subcortical areas. SC-superior colliculs. LGN-lateral geniculate nucleus. CC-corpus callosum. FC-frontal cortex. AC-anterior commissure. NF-m-neurofilament-m. GAPDH-metabolic protein used as loading control.

This microdissection technique was validated by conducting a western blot and testing for axonal protein enrichment in the fiber pathways compared to cortical tissue and other

subcortical regions such as the LGN and SC. As shown in **figure 13**. we observed enrichment of axonal proteins such as NF-m and Tau in corpus callosum and anterior commissure samples when compared to the SC, LGN and frontal cortex. This result supported our dissection technique, validating our corpus callosum and anterior commissure samples were primarily axonal projections.

3.3.2.2 Injection Validation:

After our dissection validation, we conducted injection validations. Since injections were conducted by hand, without stereotaxical equipment, the variation of injections was unknown initially. In order to validate our injections, we conducted western blots and incubated for all biotinylated proteins with anti-biotin antibodies. We conducted injections with a vehicle control, containing DMSO and Fast Green and validated with a western blot, as seen in **figure 14. B** to control for the solvent. This shows that no biotinylated proteins are present with the exception of endogenous carboxylases that use biotin as a cofactor. The primary bands in the vehicle control blot (**figure 14. B.**) are pyruvate carboxylase and β-methylcrtonyl CoA. As seen in **figure 14. F** there is significant signal in the cortical and corpus callosum tissues, with increased enrichment in ipsilateral hemispheres, as expected. These results both validated the success of the individual injection as well as the lack of contamination during the dissection. However, as seen in **figure 14. D**, this figure represents a "bad" injection, where NHS-Biotin was unsuccessfully injected into the cortex of the rat pup. Due to the size of the rat pup brains at p3, injections were easily faulted by either injecting too deep into the brain and adding the NHS-Biotin into to the ventricle or too shallow and not penetrating the dura. Furthermore, if the vehicle was injected too quickly or the micropipette was removed too quickly, the NHS-Biotin would exsanguinate from the

Graph 1 Quantification of biotinylated proteins via imagej analysis of western blots from various litters. CL-ipsilateral cortex. CR-contralateral cortex. CCL-ipsilateral corpus callosum. CCR-contralateral corpus callosum. Controls samples injected with DMSO and Fast Green. Starts indicate the samples sent for mass spectrometry.

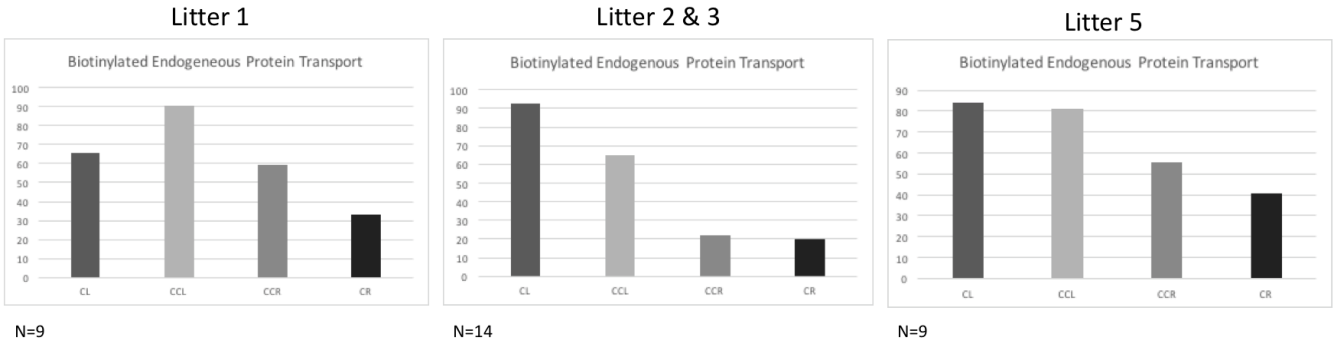

brain. These challenges arose in 15% of injections, therefore this validation step was critical before further analysis. Similarly to immunohistochemistry, endogenous carboxylases create a significant background signal. Pyruvate carboxylase is the highest enriched protein in tissue that creates this artificial signal. However, because we know the molecular weight of pyruvate carboxylase it is easily distinguishable from the signal of endogenous biotinylated proteins.

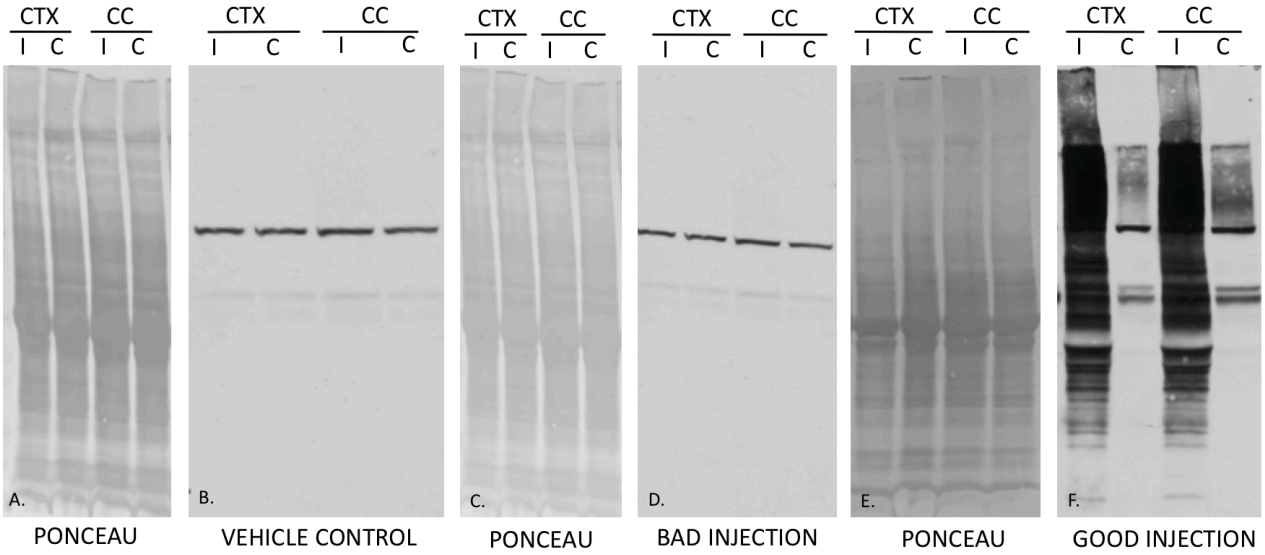

Figure. 14 Western Blots to evaluate injection validity. CTX-cortex. CC-corpus callosum. I-ipsilateral. C-contralateral. **A.** Ponceau stain used as loading control for figure b. **B.** Vehicle control, animal injected with DMSO and Fast Green, no NHS-Biotin. **C.** Ponceau stain used as loading control for figure d. **D.** Unsuccessful injection of NHS-Biotin, signal bands are endogenous carboxylases with biotin co-factor. No biotinylation of endogenous proteins. **E.** Ponceau stain used as loading control for figure f. **F.** Valid injection of NHS-Biotin, with significant ipsilateral biotinylated endogenous protein signal with signal present in contralateral hemisphere.

Furthermore, a step could be added prior to the immunoprecipitation of biotin via streptavidin beads. Using beads conjugated with an anti-pyruvate carboxylase antibody, these proteins can potentially be reduced 100 fold, resulting in the significant decrease in background signal in both biochemistry studies and mass spectrometry evaluation

Tissue from each animal after dissection was incubated for biotin, as seen in **figure 14. F**, for injection validation purposes. Using imageJ, the biotinylated signal was quantified for each animal. Averaging the approximate biotinylation signal within each litter, **Graph 1** was created to represent the population of biotinylated proteins within each dissected structure. Animals that showed greater presence of biotinylated proteins in contralateral samples than ipsilateral samples were not used for biochemical or mass spectrometry studies, due to potential contamination. The biotinylated signal is highest on the ipsilateral side due to the proximity of the injection. As the biotinylated proteins are transported the magnitude decreases. However, the presence of biotinylated proteins in the contralateral samples validates this technique for long-range projections in the brain. This technique was successfully applied to circuits outside of the visual system.

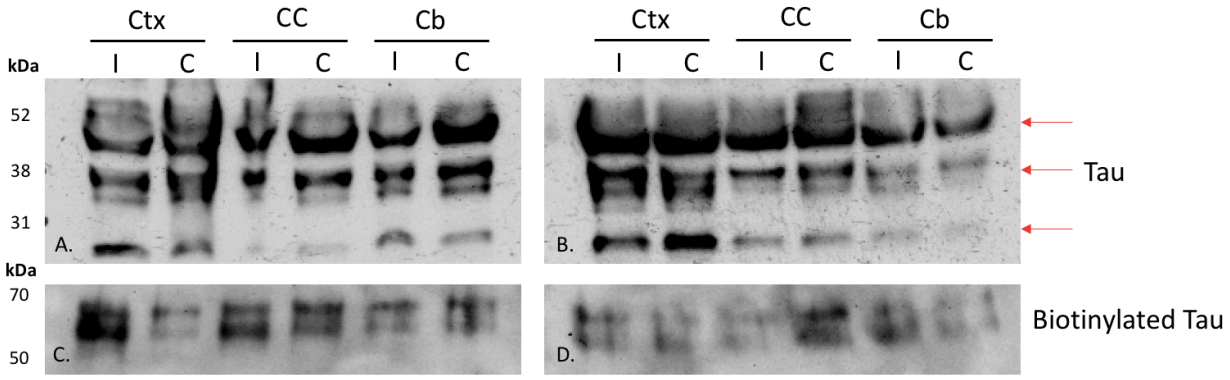

Figure. 15 Ctx-cortex. CC-corpus callosum. Cb-cerebellum. I-ipsilateral. C-contralateral. **A. B.** Inputs of Tau show consistent endogenous expression across all samples. **C. D.**Western blot of biotinylated Tau, purified by immunoprecipitation using high capacity streptavidin beads. Western blots were probed with mouse anti-Tau. **A. C.** First replicate from same pup. **B. D.** Second replicate from same pup.

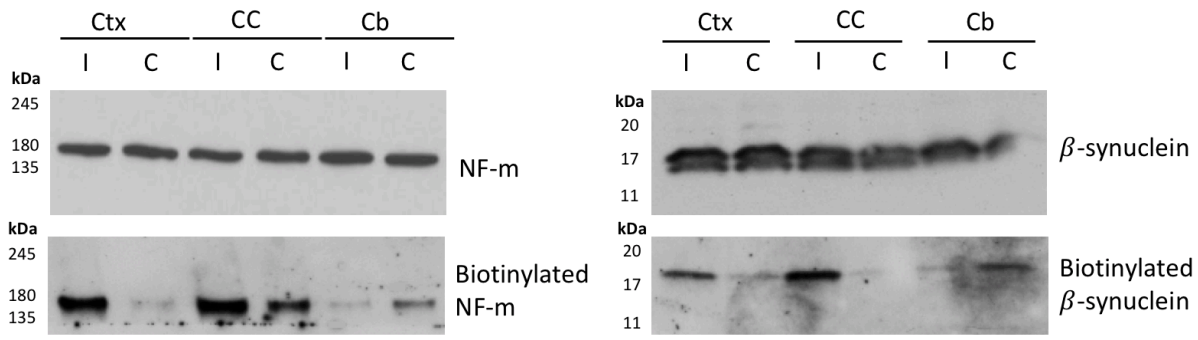

Figure. 16 Ctx-cortex. CC-corpus callosum. Cb-cerebellum. I-ipsilateral. C-contralateral. **A.** NF-m and **B.** β-synuclein input to show consistent expression across samples. **C.** Immunoprecipitated biotinylated proteins using streptavidin beads, incubated for NF-m. **D.** Immunoprecipitated biotinylated proteins using streptavidin bead, inclubated for β-synuclein.

After the validation of both the dissection strategy and the injection strategy we immunoprecipitated the biotinylated endogenous proteins with streptavidin conjugated beads. First from the initial homogenized samples we ran an input control to measure consistent expression of our axonal candidates; Tau, NF-m and β-synuclein. In **figure 15.A** and **B**, replicates from two different animals, show relative equal expression of Tau between dissected samples. In **figure 15. C** and **D**, the homogenates were incubated with streptavidin beads to immunoprecipitate all biotinylated proteins. From this enriched sample, the western blot was incubated with anti-Tau antibodies to probe for the biotinylated Tau (**Fig. 15. C and D**). In this blot we see biotinylated Tau enriched in the ipsilateral samples, as expected, due to the vicinity to the injection site. The corpus callosum samples, ipsilateral and contralateral, have relatively equal intensity due to the rate of transport across this axonal pathway. Further, the corpus callosum is highly dense in axons with increased levels of Tau compared to cortical tissue.

In **figure 16. A**, the inputs of NF-m across dissected samples is consistent to compare against the biotinylated NF-m proteins. In **figure 16. B**, we see significant enriched signal in ipsilateral samples. This finding is consistent with the biotinylated Tau data and our assumptions about increased labeling at the injection site. There is signal present in the contralateral samples,

indicating the transport of biotinylated endogenous NF-m from the ipsilateral cortex to the contralateral hemisphere. Similarly, to biotinylated Tau we see relative intensity between ipsilateral and contralateral corpus callosum samples. Lastly, we see biotinylated NF-m present in the contralateral cerebellum sample. The presence of biotinylated protein in the contralateral cerebellum is consistent with the cortico-spinal tract projection. The CST crosses hemispheres before projecting to the spinal cord and is why no signal can be detected in the ipsilateral cerebellum.

The last axonal candidate investigated by western blot was β-synuclein. **Figure 16. C**, are the inputs of β-synuclein across dissected samples. **Figure 16. D** show the same results as the previous axonal candidates. However, the lack of signal in the contralateral corpus callosum was due to processing error, because there is signal present in the contralateral cortex. These experiments validate the colocalization experiments conducted with immunohistochemistry. These results show that the endogenous biotinylated protein is successfully transported and visualized. Therefore, with these results we can further investigate the population of the transportome in these long-range projections.

3.3.3 Mass Spectrometry Evaluation

Table 1 Quantification of protein input for each mass spectrometry sample during processing to dictate pooling of samples after precipitation.

Replicate	Ipsi – Cortex	Ipsi – Corpus Callosum	Contra – Corpus Callosum	Contra – Cortex
1	25 mg	15 mg	15 mg	25 mg
2	15 mg	10 mg	10 mg	15 mg
3	10 mg	5 mg	15 mg	10 mg
Control (DMSO)	15 mg	15 mg	15 mg	5 mg

To investigate the transportome across intercortical pathways with high throughput, we used mass spectrometry to identify this population. We conducted injections in a similar fashion as the histochemical and biochemical studies. The dissected tissue homogenate was further

processed using the developed DiDBiT strategy. This method as previously discussed allows for significantly higher sensitivity than conventional methods. The four main processing steps included; precipitation, desalting, digestion and enrichment. The precipitation step allowed us to pool significant tissue samples, while reducing solvent volume. After quantifying the protein concentration for each tissue sample, using Bradford assays and validating each injection via western blot, we combined samples from the same litter to reach 5 mg protein samples. We further combined samples to have a range of input concentrations to assess the efficiency of the mass spectrometry readouts, ranging from 5 mg to 25 mg. After using a common chloroform and methanol precipitation method, the samples were desalted using an immobilized silica column. Drying the elution after each step for 2 hours using a vacuum evaporator. With the precipitated, dried sample we used 8 M Urea to resuspend our proteins to continue to the digestion stage. As mentioned previously by digesting the protein before enrichment we drastically reduce

Graph 2 Peptide Quantification after protein digestion for each sample. Red bars indicate one week trypsin digestion. Blue bars indicate 24 hour trypsin digestion. XL-ipsilateral cortex. XR-contralateral cortex. CCL-ipsilateral corpus callosum. CCR-contralateral corpus callosum. Controls samples injected with DMSO and Fast Green. Starts indicate the samples sent for mass spectrometry.

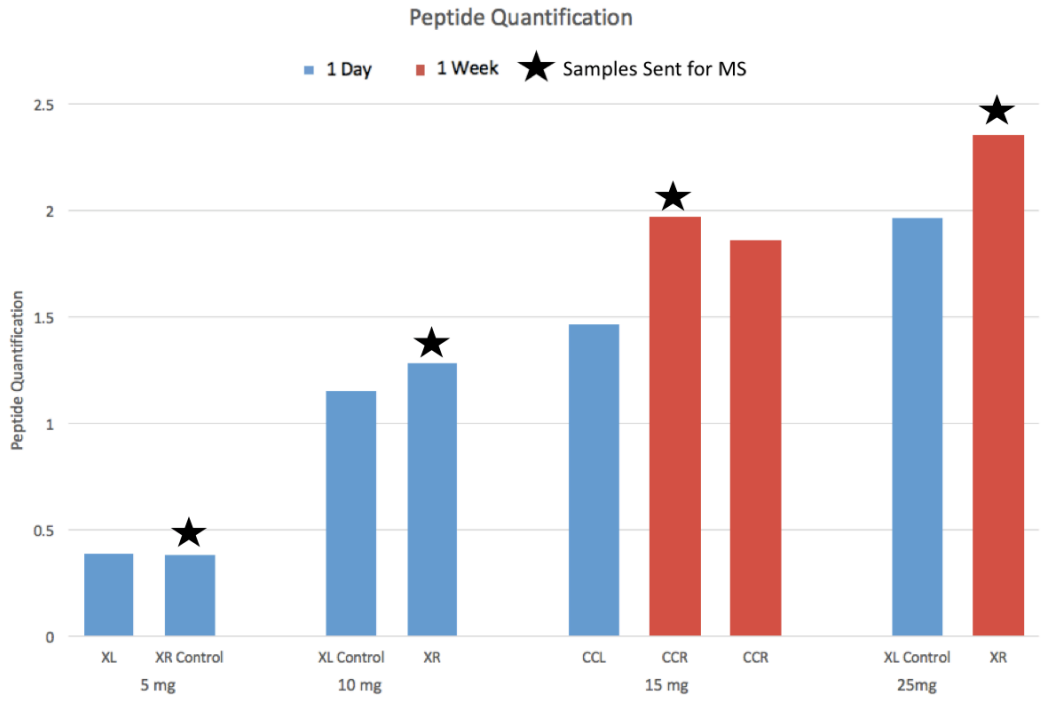

contamination by non-specific binding of proteins that may have affinities to the biotinylated proteins. The trypsin digestion is a common protocol for mass spectrometry and has been previously validated as a successful technique. We also varied the time in which we incubated the digestion; one day and one week digestions. To validate the digestion of the proteins we conducted a peptide quantification assay. We observed that the one week digestion improved the peptide quantity but not significantly (**Graph 2**). As seen in **graph 2**, with increasing protein input, there was an increasing trend in peptide quantity. The first four samples sent to mass spectrometry were contralateral samples (indicated by the stars in **graph 2**); one contralateral cortex control, two contralateral cortex samples and one contralateral corpus callosum. Prior to

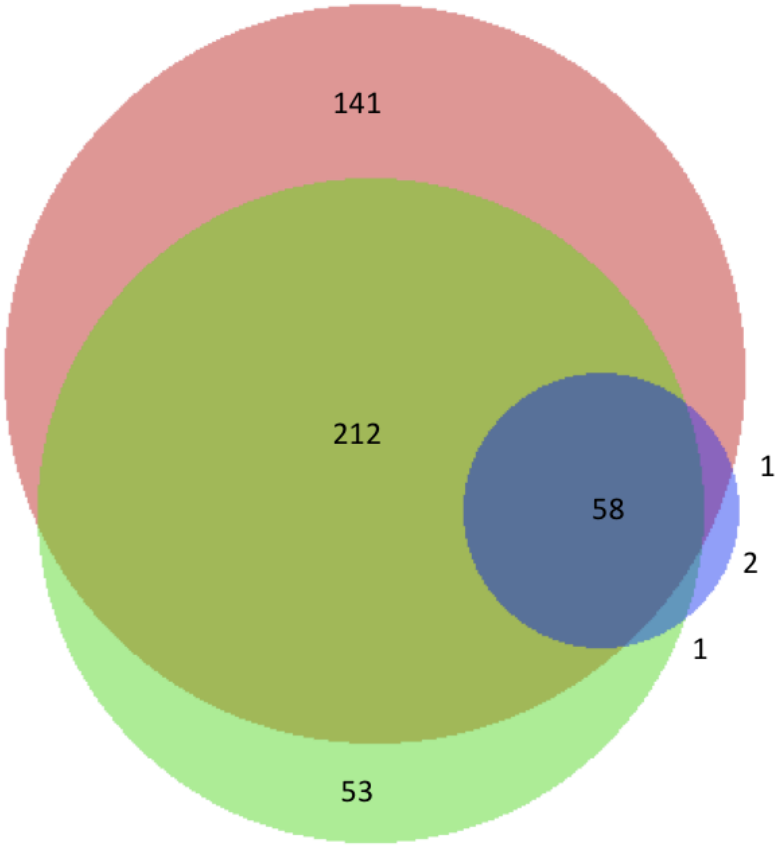

Figure. 17 Venn Diagram of Biotinylated Protein Counts from Mass Spectrometry. Green Circle: Contralateral Cortex sample with 10 mg input. Red circle: Contralateral Cortex sample with 25 mg input. Blue circle: Contralateral Corpus Callosum sample with 15 mg input.

analysis, we enriched the peptides with Neutravidin high capacity beads. With the peptide sample resuspended in PBS, we incubated the peptides with the Neutravidin beads overnight at 4℃, and eluted the enriched peptides. This sample was washed and sent for analysis.

Our results from mass spectrometry showed significant counts of a wide range of proteins within the developing rodent brain. The fascinating data set counted 400+ proteins for the cortical samples, 64 proteins in the corpus callosum sample, and 9 proteins for the DMSO injected control sample. The control sample validated our experiment because all proteins identified use biotin as a cofactor, such as pyruvate carboxylase, seen previously in the biochemical studies. The high count of this background signal could pose issues that skew the spectrometry counts of the other significant proteins in the injected samples. In future sample preparation, we will use methods such as immunoprecipitation to target these contaminating proteins to potentially increase the sensitivity of the readout of the samples. All significant proteins that were found in the corpus callosum were also present in the contralateral cortex (**figure 17**). There were 406 proteins present in the contralateral cortical samples that were identified in the UniProt sequence database, and 58 were found to be in all three samples. Only 2 proteins were found to be only transported to the corpus callosum but not present in the contralateral cortex; cytochrome b561 and Versican Core Protein (Vcan). Vcan is a chondritin sulfate proteoglycan, which has been implicated in callosal development in previous literature (Milev et al, 1998). Several other glycoproteins were identified and have been implicated in neuronal development. Neuronal membrane glycoprotein (Gpm6a), in previous studies, has been shown to induce neurite extension, a major function in synaptic plasticity (Alfonso et al, 2005). Syndecan-2 has similar roles in the developing rodent brain, although there was no sequence

count for this protein, CASK was found in our contralateral cortical sample. CASK is the binding partner of syndecan-2 and known to induce dendritic spine morphological changes leading to development of synapses and plasticity later in life (Yamaguchi 2001). These results are validated by the developmental time point of the rats; synaptic development is predominantly occurring p8-p15 for the axons projecting across the corpus callosum and other long range fiber tracts.

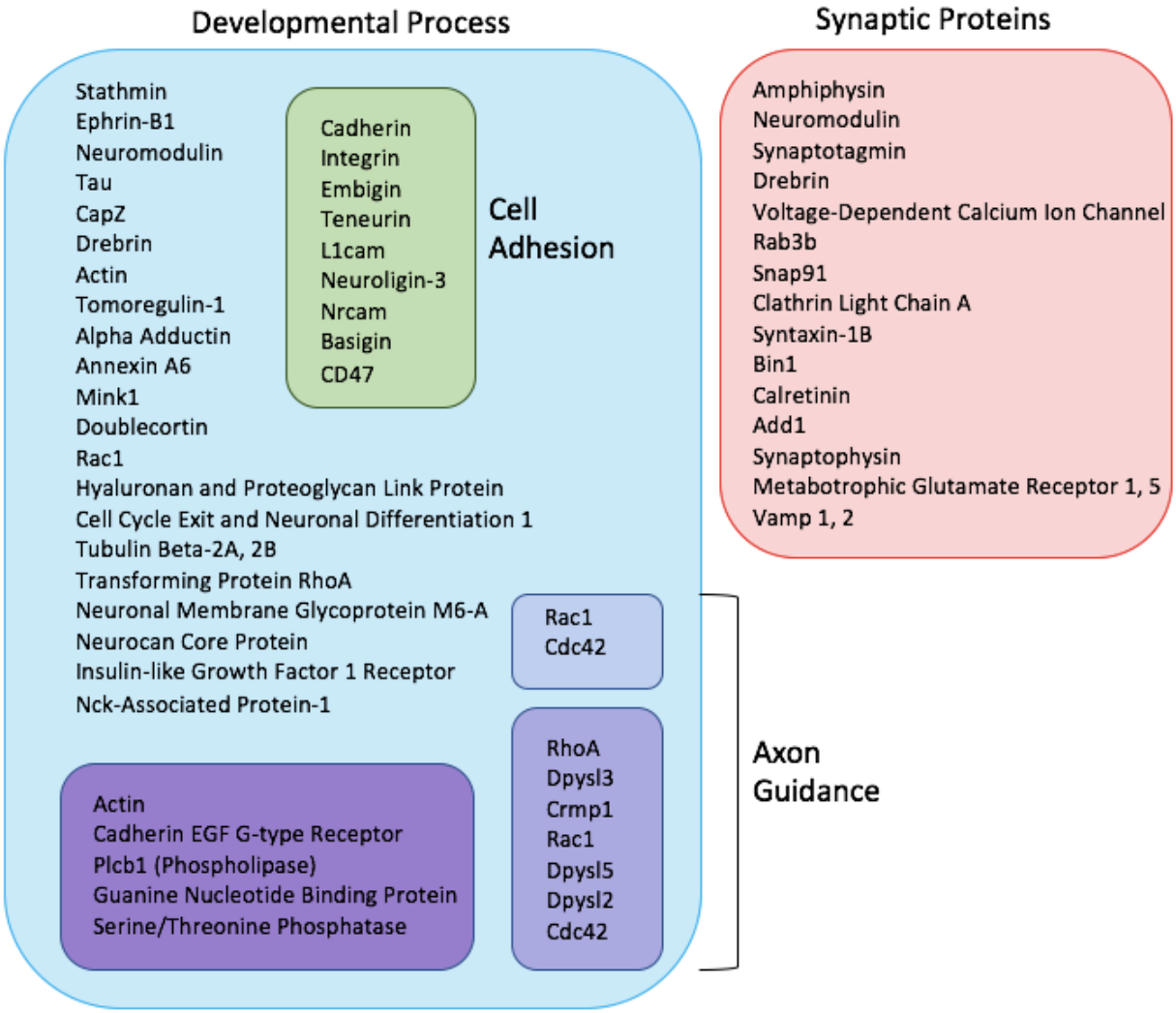

Figure. 18 Mass Spectrometry Reads of Proteins Biotinylated in Contralateral Cortex. Protein function sorted with PANTHER. Blue Box: Proteins Involved in Developmental Processes. Red Box: Synaptic Proteins Purple Boxes: Axon Guidance (light: Slit/Robo and Netrin signaling, medium: Semaphorin mediated signaling, dark: Wnt signaling).

The class of proteins that were found to be the highest prevalence among the biotinylated transported proteins were cell adhesion molecules, as seen in the green box of **figure 18**. Furthermore, many cellular process enzymes were present in high concentrations, such as glycolytic and cellular respiration enzymes. The cell adhesion molecule with the most significant spectrometric count was Neural Cell Adhesion Molecule (Nrcam), a vital axon guidance and synaptic development cue. Due to its vitality in development, Nrcam has been implicated with neurodevelopmental disorder such as Autism, when mutated or epigentically down-regulated. Furthermore, Nrcam regulates downstream effector semaphorin 3F (Sema3F), associated with dendritic spine formation and pruning (Demyanenko et al, 2014). Due to the role in axon guidance during development, these proteins are vital for the interhemispheric pathway formation and could augment the compiled data regarding the complexity of the regulation of fiber tract development. In addition to the prominent semaphorin family of guidance molecules, ephrins are vital to the proper formation of all fiber tracts. Our mass spectrometry data showed many proteoglycan molecules that were biotinylated and have been observed in previous studies to coordinate ephrin signaling. As seen in **figure 18**, EphB2 was found to be transported from the ipsilateral cortex to the contralateral cortex. EphB2 is necessary for the proper formation of the corpus callosum and the anterior commissure in the developing brain. Mutation studies have shown that when this receptor is truncated or knocked out entirely, there are severe misprojections of commissural axons as well as significant agenesis of these fiber pathways (Robichaux et al, 2016).

We hope to conduct similar biochemical studies and perform immunoprecipitation assays with streptavidin conjugated agarose beads. We will probe for candidates; Nrcam, EphB1 and Sema3F to validate the biotinylation and therefore transport of these guidance molecules across

callosal fibers to the contralateral cortical tissue. As proteoglycans have been highly implicated in our mass spectrometry data and previous literature suggests their prominent role in neural development, it would be interesting to investigate individual proteoglycans such as Vcan and Neurocan. We intend for these results to not only validate our mass spectrometry findings but quantify the differential expression and transport across the callosal fiber pathway to the contralateral cortex. We will further use immunohistochemistry to visualize the expression of these axon guidance molecules.

The next step of this project will be to reproduce these experiments but during various developmental time points. It will be interesting to analyze the differential expression of these axon guidance molecules and cell adhesion molecules post-natal day 1, when neurite extension is predominant, as well as p14 when synaptic formation and refinement is prevalent. Lastly, conducting mutagenic studies to knockdown or knockout the previously mentioned candidates will be fascinating to determine their significance in neural circuit development.

Chapter 4: Conclusion and Future Directions

The purpose of this paper was to apply the NHS-Biotin labeling strategy to the developing rodent brain to investigate the intercortical and subcortical protein transport in long range axonal projections. NHS-Biotin overcomes many limitations posed by previous labeling strategies and the versatility allows for investigation by immunohistochemistry, biochemistry, mass spectrometry and electron microscopy. Although this paper only reviews the first three modes of analysis, we have accumulated significant data that identifies the subpopulation of the proteins transported along these fiber tracts. Using immunohistochemical analysis, we visualized both at a mesoscale and microscale, the interconnectivity of the developing rodent brain and

trace biotinylated endogenous protein in long range projections, specifically, the cortico-spinal tract, the corpus callosum and anterior commissure. Probing for individual candidates we localized the endogenous biotinylated signal with axonal and synaptic proteins, such as Tau and synapsin. We observed single axonal projections protruding from the contralateral corpus callosum to synapse in the contralateral cortex. To validate these findings, we conducted biochemical assays to definitively probe for these biotinylated axonal and synaptic proteins via western blots. By conducting immunoprecipitation of the dissected tissue lysate, we enriched the samples to isolate only the labeled protein. We observed significant signal of biotinylated Tau and NF-m in the ipsilateral samples but also observed signal in the contralateral samples, indicating the successful transport of these axonal proteins that were biotinylated at the site of injection and transported anterogradely towards the developing synapses.

Lastly, using the DiDBiT strategy developed by the Cline lab, we analyzed the biotinylated samples via mass spectrometry to identify the entire population of the transportome. We primarily investigated the contralateral cortex and corpus callosum, as these axonal projections were the most significant to our research, rather than the cellular labeling of the ipsilateral cortex. With higher sensitivity than conventional digestion methods we produced a sample of biotinylated peptides with minimal contamination from non-specific interactions and associated protein complexes. Therefore, we had high confidence in the results we achieved from mass spectrometry. The biotinylated proteins of the highest relevance to our data set were cell adhesion molecules, synaptic proteins, and axon guidance signaling molecules. Using PANTHER, we sorted the list of 418 proteins by several factors; cellular localization, biological process, molecular function, and signaling pathway. The cell adhesion molecules had the highest sequence counts and secondly, proteoglycans involved in axon guidance signaling.

Commissures in the evolved brain have been implicated with increased wiring accuracy and reduction of misprojections, both in intrahemispheric and interhemispheric connections (Comer et al, 2019). In future studies, NHS-Biotin injections can be used to further evaluate the intricate signaling pathways that establish these commissures as well as how these commissures induce proper wiring of axonal projections. The four protein families of axon guidance molecules; Slits, Netrins, Ephrins and Semaphorins all play significant roles in nearly every stage in development from neurite extension and guidance to synaptic formation (Comer et al, 2019). Previous studies have highlighted the individual protein's influence on one aspect of development but no studies have exhaustively investigated the role of an entire axon guidance protein family. This labeling strategy can be used investigate the missing pieces of fiber tract development, in the future. This data set of transported proteins in the developing rodent brain can be used to compare future datasets from transgenic or mutagenic studies or at various time points. This paper serves to prove that NHS-Biotin can be used as a labeling technique for long-range projections *in vivo* and future studies can use this dataset as a baseline for the normal developing rodent model.

APPENDIX

Supplementary Figures:

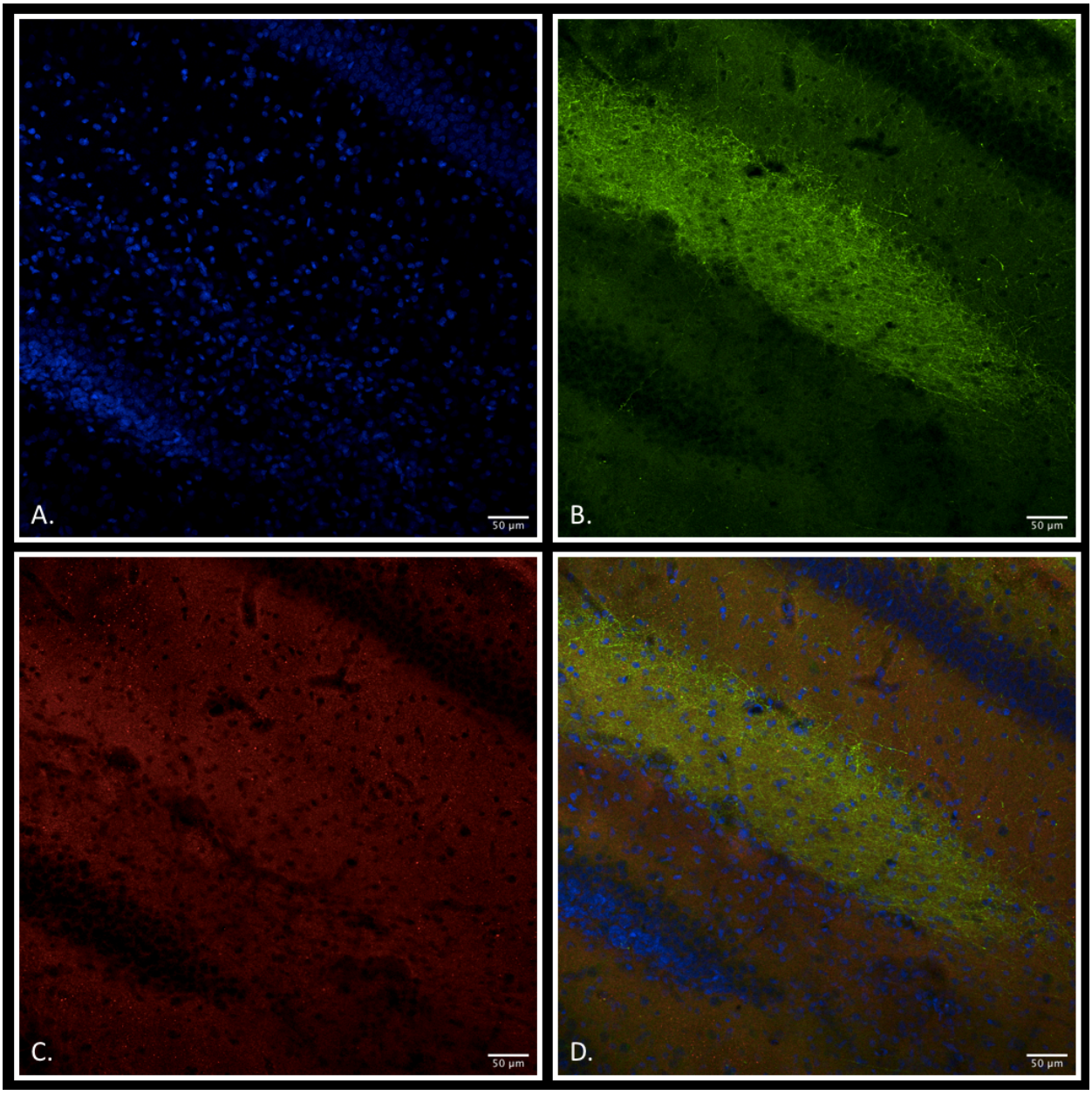

Supplementary Figure 1 Contralateral hippocampus of p8 mouse pup after p3 unilateral intercortical NHS-Biotin injection. **A.** DAPI. **B.** Biotinylated endogenous proteins immunostained with goat anti-biotin. **C.** Tau visualized with mouse anti-tau. **D.** Composite image of a. b. and c.

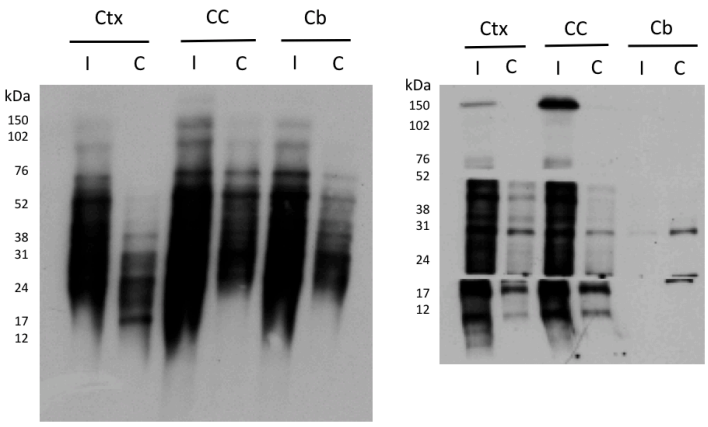

Supplementary Figure 2 Injection Validation Western Blots. Dissected sample lysates incubated for biotinylated proteins. I-ipsilateral, C-contralateral. Ctx-Cortex, CC-corpus callosum, Cb-cerebellum. These two animals also represented "good" injections.

Supplementary Graph 1 Biotin detection assay of protein inputs for mass spectrometry. The Contra-Cortex Control (vehicle control) shows higher levels of biotin quantification than the contra-cortex replicate 1. We switched to the peptide quantification assay because this particular assay was unreliable.

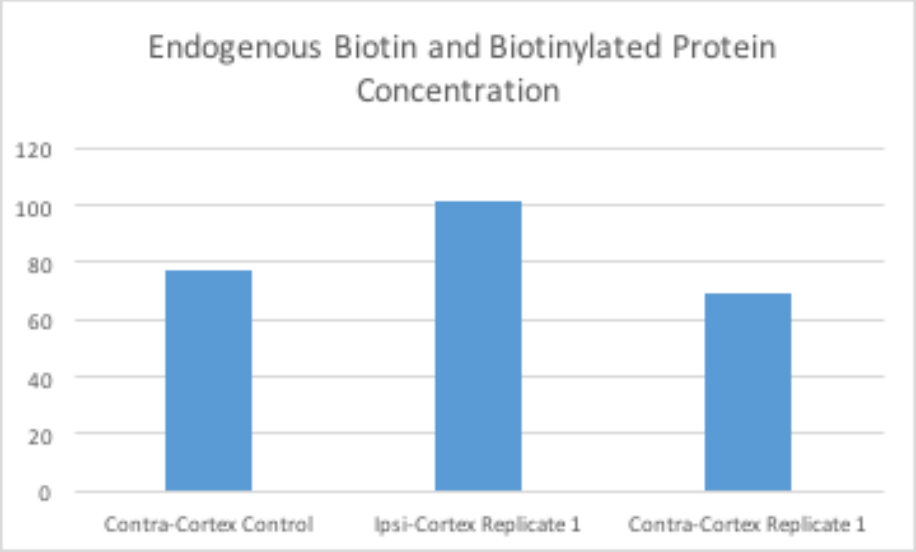

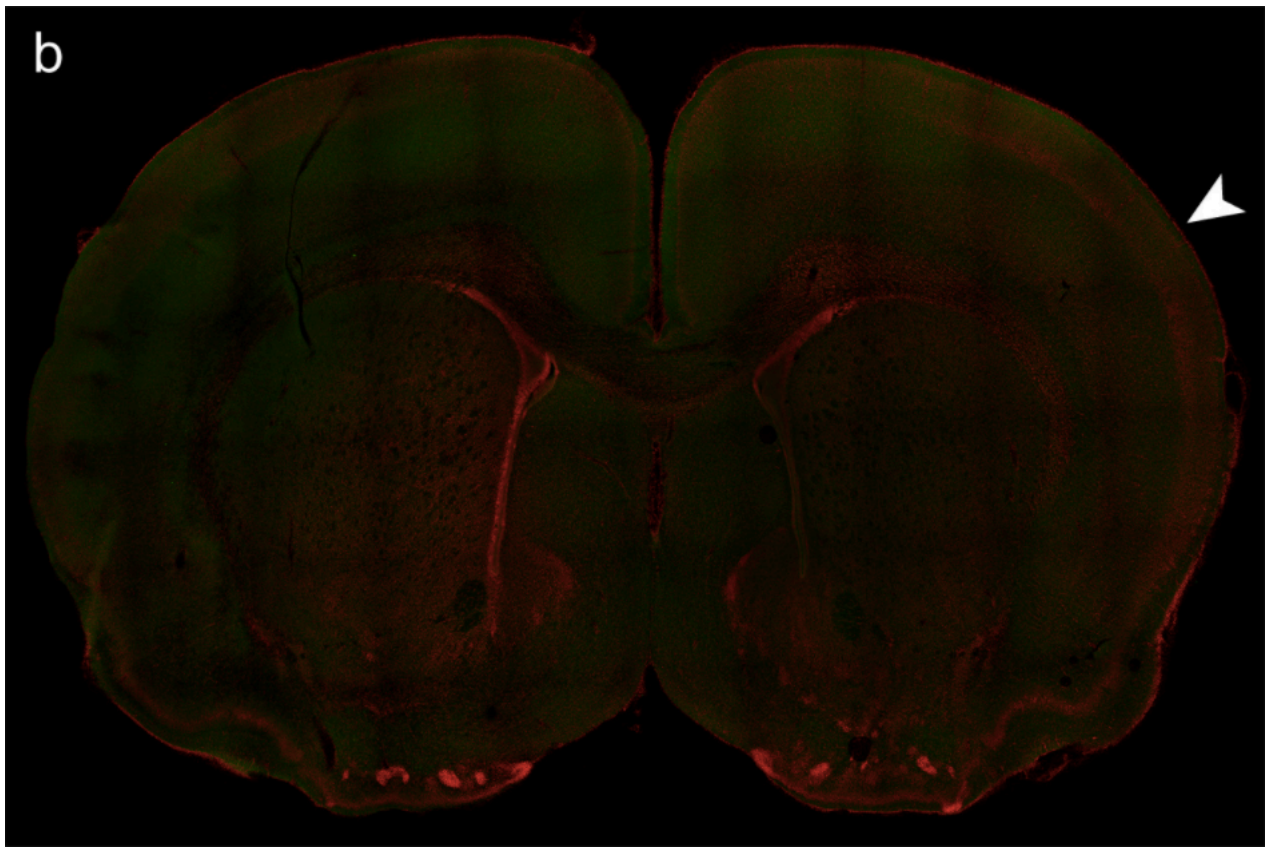

Supplementary Figure 3. Whole brain image of p8 mouse pup, vehicle control (DMSO).

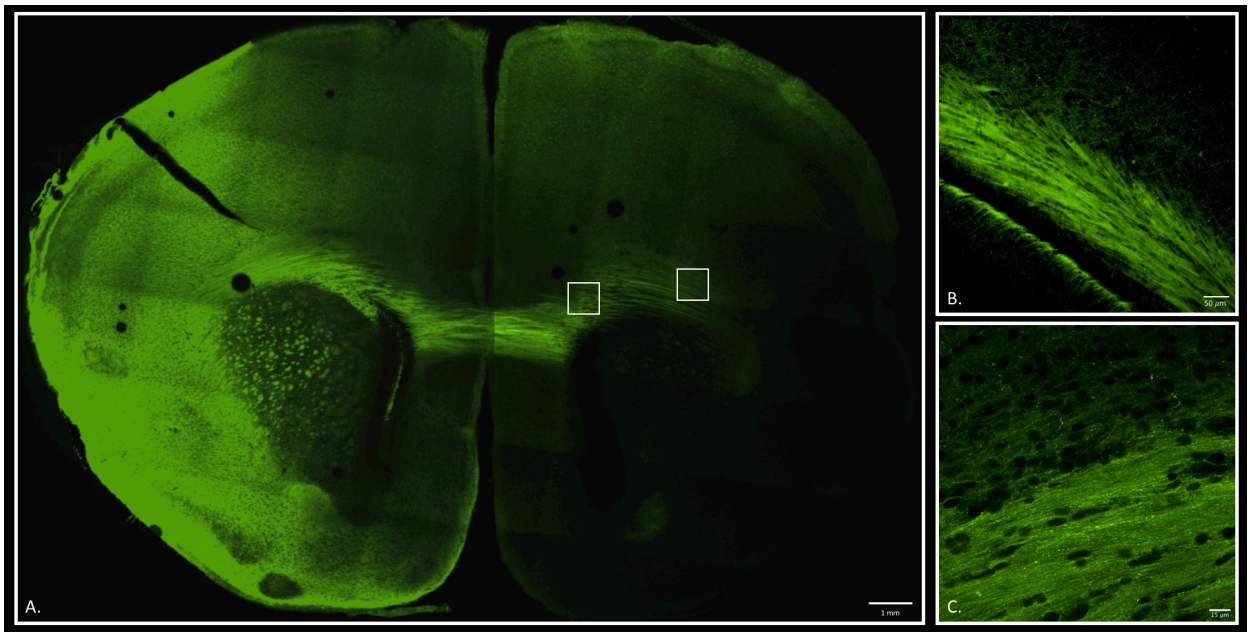

Supplementary Figure 4 A. Whole brain image of p4 mouse pup. B. contralateral corpus callosum, 20X magnification. C. Contralateral corpus callosum, 40X magnification.

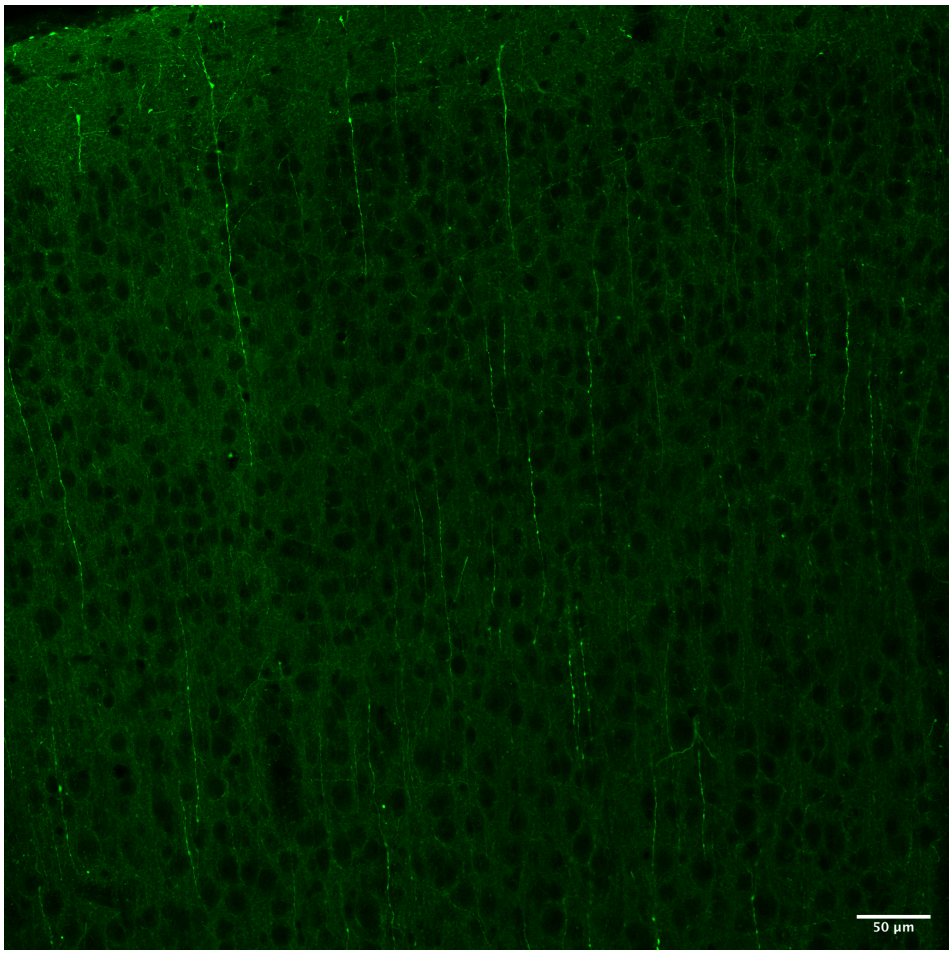

Supplementary Figure 5 Contralateral Cortex of p8 mouse, 20X. Green-Biotin

Supplementary Table 1 Mass Spectrometry Data for Contralateral Corpus Callosum Sample.

Accession Number	Gene Name	Spec Count
P13596;	Ncam1	74
P02770;	Alb	37
P68370;Q6P9V9;Q68FR8;	Tuba	20
P52873;	Pc	19
Q63198;	Cntn1	17
P07340;	Atp1b1	13
P47942;	Dpysl2	12
P60711;P63259;	Act	10
P15999;	Atp5a1	8
P32736-2;P32736;	Ocpml	7
P04797;	Gapdh	6
P19332-2;	Mapt	6
P04764;	Eno1	6
P15431;P63138;P63079;	Gabrb	6
P55067;	Ncan	6
P07936;	Gap43	5
P10111;	Ppia	5
P04636;	Mdh2	5
P10719;	Atp5b	5
Q9WUC4;	Atox1	4
P31000;	Vim	4
Q794F9;	Slc3a2	4
Q05962;	Slc25a4	3
O88767;	Park7	3
Q05175;	Basp1	3
Q9ERB4-2;Q9ERB4;Q9ERB4-3;	Vcan	3
P50398;	Gdi1	3
Q63416;	Itih3	3
P97685-2;P97685;P97685-3;	Nfasc	3
P63102;	Ywhaz	2
P11232;	Txn	2
P45592;	Cfl1	2
P55051;	Fabp7	2
Q09073;	Slc25a5	2
P10888;	Cox4i1	2
Q812E9-2;Q812E9;	Gpm6a	2
P50137;	Tkt	2
Q62950;	Crmp1	2
Q9R066-2;Q9R066;	Cxadr	2
Q64559-2;Q64559;	Acot7	2
Q9Z0J8;	Negr1	2
P23565;	Ina	2
P62630;	Eef1a1	2
O35276;	Nrp2	2
P30904;	Mif	1
Q641Y1;	Cyb561d2	1
P01835;P01836;		1
P61354;	Rpl27	1
P04218;	Cd200	1
Q06647;	Atp5o	1
Q4QRB4;	Tubb3	1
O88989;	Mdh1	1
P35435;	Atp5c1	1
P63018;	Hspa8	1
P14882;	Pcca	1
P63039;	Hspd1	1
P41562;	Idh1	1
Q9ER34;	Aco2	1
Q05695-2;Q05695;	L1cam	1
P85845;	Fscn1	1
P31422;	Grm3	1
P11442;	Cltc	1

Supplementary Table 2 Mass Spectrometry Data for Contralateral Cortex (10 mg) Sample.

Accession Number	Gene Name	Spec Count
P13596;	Ncam1	282
Q63198;	Cntn1	121
P68370;Q6P9V9;Q68FR8;	Tuba1	99
P02770;	Alb	94
P19332-2;	Mapt	78
P07936;	Gap43	77
P15865;	Hist1h1e	75
P60711;P63259;	Act	60
P04797;	Gapdh	57
Q5XIF6;	Tuba4a	47
P47942;	Dpysl2	44
P04764;	Eno1	41
Q62950;	Crmp1	40
D3ZBN0;	Hist1h1b	37
P04636;	Mdh2	37
P07340;	Atp1b1	36
P15999;	Atp5a1	36
P63039;	Hspd1	32
P10719;	Atp5b	32
Q05175;	Basp1	31
Q62718;	Ntm	31
P32736-2;P32736;	Opcml	29
P63102;	Ywhaz	28
P10111;	Ppia	27
P55051;	Fabp7	27
P45592;	Cfl1	27
Q9ERB4-2;Q9ERB4;	Vcan	27
Q05962;	Slc25a4	25
P04218;	Cd200	25
Q62813-2;Q62813;	Lsamp	25
P97685;	Nfasc	24
P52873;	Pc	24
Q05695-2;Q05695;	L1cam	23
P35213-2;P35213;	Ywhab	22
P31000;	Vim	22
Q6P6R2;	Dld	22
P26772;	Hspe1	21
Q9ER34;	Aco2	21
P54290;	Cacna2d1	21
P00507;	Got2	20
B3GNI6-2;B3GNI6;B3GNI6	11-Sep	20
P59215;	Gnao1	20
P17764;	Acat1	18
P16617;	Pgk1	18
P55067;	Ncan	18
P11030;	Dbi	17
O88989;	Mdh1	17
P68255;	Ywhaq	17
Q09073;	Slc25a5	17
P62630;	Eef1a1	17
P50137;	Tkt	17
P06687;	Atp1a3	17
Q62656-2;Q62656;Q62656	Ptprz1	17
P31399;	Atp5h	16
P13086;	Suclg1	16
O88767;	Park7	15
P62260;	Ywhae	15
P97603;	Neo1	15
Q63416;	Itih3	15
Q06647;	Atp5o	14
Q9Z0J8;	Negr1	14
P25113;	Pgam1	13
Q794F9;	Slc3a2	13
P07335;	Ckb	13
P48500;	Tpi1	12
P11442;	Cltc	12
Q00981;	Uchl1	11
P61765-2;P61765;	Stxbp1	11

Supplementary Table 2 Mass Spectrometry Data for Contralateral Cortex (25 mg) Sample, continued.

Accession Number	Supplementa Gene Name	Spec Count
P55053;	Fabp5	10
Q63507;	Rpl14	10
P61983;	Ywhag	10
P10860;	Glud1	10
Q63754;	Sncb	9
P37377-2;P37377;	Snca	9
Q64361;	Lxn	9
Q9JHU0;	Dpysl5	9
Q9R066-2;	Cxadr	9
P62845;	Rps15	9
P35053;	Gpc1	9
P15431;P63138;P63079;	Gabrb	9
P29418;	Atp5e	8
Q03344;	Atpif1	8
B2GV06;	Oxct1	8
P56574;	Idh2	8
P23565;	Ina	8
P85845;	Fscn1	8
Q64428;	Hadha	8
P16036;	Slc25a3	8
Q9WVC0;	7-Sep	8
Q4V887;	Slc39a6	8
Q4QRB4;	Tubb3	8
Q3KRE8;	Tubb2b	8
P46101-2;P46101;	Dpp6	8
P13668;	Stmn1	7
Q9EPH2;	Marcksl1	7
O35244;	Prdx6	7
Q1WIM3;	Cadm3	7
Q6MG60;	Ddah2	7
Q8VHF5;	Cs	7
O35112;	Alcam	7
P14408-2;P14408;	Fh	7
O08875;	Dclk1	7
P47858;	Pfkm	5
O88871;	Gabbr2	5
P62898;	Cycs	4

Accession Number	Gene Name	Spec Count
P97686-2	Nrcam	7
P23693	Tnni3	7
P04905;	Gstm1	6
D3ZW55;	Itpa	6
Q99NA5;	Idh3a	6
P32551;	Uqcrc2	6
P10888;	Cox4i1	6
Q920L2;	Sdha	6
P85834;	Tufm	6
P69897;	Tubb5	6
P31422;	Grm3	6
O35276;	Nrp2	6
Q62952-2;Q62952;	Dpysl3	6
Q1WIM2-2;Q1WIM2;	Cadm2	6
P14882;	Pcca	6
Q9R1Z0-2;Q9R1Z0;	Vdac3	5
P42123;	Ldhb	5
P97710;	Sirpa	5
Q9WVK7;	Hadh	5
Q63135-2;Q63135;	Cr1l	5
P05708;	Hk1	5
P11884;	Aldh2	5
Q505J6;	Slc25a18	5
Q99MZ8;	Lasp1	5
Q68FR6;	Eef1g	5
P51635;	Akr1a1	5
P19511;	Atp5f1	5
P25286-2;P25286;	Atp6v0a1	5
Q3KR86;	Immt	5
P32851;P61265;	Stx1	5
P50398;	Gdi1	5
Q5FVJ0-2;Q5FVJ0;	Rufy3	5
P0C2X9;	Aldh4a1	5
P31596-2;P31596;	Slc1a2	5
P11240;	Cox5a	3
P61354;	Rpl27	3
P52759;	Hrsp12	3

Supplementary Table 2 Mass Spectrometry Data for Contralateral Cortex (10 mg) Sample, continued.

Accession Number	Gene Name	Spec Count
Q9EPC6;	Pfn2	4
P63159;	Hmgb1	4
Q9WUC4;	Atox1	4
P05065;	Aldoa	4
Q8CFN2-2;Q8CFN2;	Cdc42	4
P11232;	Txn	4
P47727;	Cbr1	4
P27274;	Cd59	4
P54311;	Gnb1	4
P63025;Q63666;	Vamp	4
P67779;	Phb	4
P18420;	Psma1	4
P63018;	Hspa8	4
P52796;	Efnb1	4
P50399;	Gdi2	4
P31044;	Pebp1	4
Q812E9-2;Q812E9;	Gpm6a	4
Q9QYV1;	Tmeff1	4
P41562;	Idh1	4
O88600;	Hspa4	4
Q64559-1;Q64559;	Acot7	4
P97527;	Cntn5	4
Q920Q0;	Palm	4
Q01205;	Dlst	4
Q9JLT0;	Myh10	4
Q6P6V0;	Gpi	4
P15146-2;P15146-3;	Map2	4
B0K020;	Cisd1	3
Q6RUV5;	Rac1	3
P25886;	Rpl29	3
P17078;	Rpl35	2
P62278;	Rps13	2
P39032;	Rpl36	2
P17074;	Rps19	2
Q5XIE6;	Hibch	2
P10536;Q6NYB7;	Rab	2
P14942;	Gsta4	2
P07825;	Syp	2

Accession Number	Gene Name	Spec Count
O70257;	Stx7	3
P11980-2;P11980;	Pkm	3
P04642;	Ldha	3
B0BNA5;	Cotl1	3
D3ZE85;	Frrs1l	3
P19527;	Nefl	3
P62749;Q5PQN0;P84076;	Hpcal1/Ncald	3
P40307;	Psmb2	3
P11598;	Pdia3	3
P61206;Q5BK71;P84083;	Arf	3
Q62609-3;Q62609;	Olfm1	3
Q5XI73;	Arhgdia	3
O35814;	Stip1	3
P14668;	Anxa5	3
P35435;	Atp5c1	3
P84092;	Ap2m1	3
P13264-2;P13264;	Gls	3
P18484;	Ap2a2	3
P21588;	Nt5e	3
P82995;	Hsp90aa1	3
Q5I0C3;	Mccc1	3
Q62889-2;Q62889;	Nlgn3	3
P97536;	Cand1	3
O88902;	Ptpn23	3
P62959;	Hint1	2
P62959;	Hint1	2
P62859;	Rps28	2
P52925;	Hmgb2	2
P04906;	Gstp1	2
Q63610-2;Q63610;	Tpm3	2
Q66HF1;	Ndufs1	2
P70627;	Folh1	2
Q05140-2;Q05140;	Snap91	2
Q9Z2L0;	Vdac1	1
P62161;	Calm1	1
Q62658;	Fkbp1a	1
Q6QI89;	Morf4l2	1
P07936	Gap43	1

Supplementary Table 2 Mass Spectrometry Data for Contralateral Cortex (10 mg) Sample, continued.

Accession Number	Gene Name	Spec Count
P21533;	Rpl6	2
P13852;	Prnp	2
Q7M0E3;	Dstn	2
Q01713;	Klf9	2
Q9EQX9;	Ube2n	2
O35264;	Pafah1b2	2
P39069;	Ak1	2
P47819-2;P47819;	Gfap	2
B0BNE5;	Esd	2
P85108;	Tubb2a	2
P21913;	Sdhb	2
Q5XI22;	Acat2	2
P23965;	Eci1	2
P24329;	Tst	2
O08651;	Phgdh	2
Q08163;	Cap1	2
Q68FY0;	Uqcrc1	2
P14740;	Dpp4	2
P38652;	Pgm1	2
Q68FX0;	Idh3B	2
P09606;	Glul	2
O88775;	Emb	2
Q5RKI0;	Wdr1	2
Q60587;	Hadhb	2
Q07266-2;Q07266;	Dbn1	2
Q499N5;	Acsf2	2
P12007;	Ivd	1
P16446;	Pitpna	1
O35331;	Pdxk	1
Q6PDU1;	Srsf2	1
Q9Z0V6;	Prdx3	1
Q9Z1B2;	Gstm5	1
Q6PCU2;	Atp6v1e1	1
Q9QYU4;	Crym	1
A0JPJ7;	Ola1	1
P21531;	Rpl3	1
P12368;	Prkar2a	1

Accession Number	Gene Name	Spec Count
P02091;P11517;	Hbb	1
P83732;	Rpl24	1
P63031;	Mpc1	1
Q62785;	Pdap1	1
P08081-2;P08081;	Clta	1
P26453-2;P26453;	Bsg	1
Q6MG61;	Clic1	1
Q3T1J1;	Eif5a	
P43278;	H1f0	1
P62828;Q8K586;	Ran/Rasl2-9	1
Q5I0M2;	Qprt	1
A9UMV8;P0CC09;	Hist2h2aa3	1
P04256;	Hnrnpa1	1
P18421;	Psmb1	1
P40112;	Psmb3	1
O70351;	Hsd17b10	1
P24368;	Ppib	1
Q63665-2	Usf2	1
P62755;	Rps6	1
Q64548-2;Q64548;	Rtn1	1
Q5M7A7;	Cnrip1	1
P47863-2;P47863;	Aqp4	1
P49911;	Anp32a	1
P62425;	Rpl7a	1
P12711;	Adh5	1
Q5XI32;	Capzb	1
P30835;	Pfkl	1
P62944-2;P62944;	Ap2b1	1
Q9Z1K9;	Adam17	1
P46462;	Vcp	1
Q5M7W5;	Map4	1
P15684;	Anpep	1
Q64663;	P2rx7	1
Q8CFG5;	Cacna2d3	1
P22063;	Cntn2	1
Q62682;	Cntn3	1
Q9Z173-2	Lphn3	1

Supplementary Table 2 Mass Spectrometry Data for Contralateral Cortex (10 mg) Sample, continued.

Accession Number	Gene Name	Spec Count
P27791-2	Prkaca	1
Q6AY23;	Pycr2	1
Q9JMJ4;	Prpf19	1
P09895;	Rpl5	1
P13437;	Acaa2	1
O35077;	Gpd1	1
Q9R080-4;	Gpsm1	1
P63095-2;	Gnas	1
Q75Q39;	Tomm70a	1
P62198;	Psmc5	1
Q63028-2;Q63028;	Add1	1
Q5XI51;Q9WV63;	Kif2	1
Q3KRE0;	Atad3	1
P13635;	Cp	1
Q66HD0;	Hsp90b1	1
Q2LC84;	Numb	1

Accession Number	Gene Name	Spec Count
P60756;	Mdga2	1
P10687;	Plcb1	1
Q8CGU4;	Agap2	1
F1LP90;	Mink1	1
Q63374-10;	Nrxn2	1
P16086;	Sptan1	1
P29994-2;	Itpr1	1
P38650;	Dync1h1	1
Q5I0G4;	Gars	1
Q9Z1A5;	Nae1	1
D3ZPX4;	Plxna3	1
Q8CFG6;	Cacna2d2	1
P49134;	Itgb1	1
O08838;Q68FR2;	Amph	1
Q9Z0U5;	Aox1	1

Supplementary Table 3 Mass Spectrometry Data for Contralateral Cortex (25 mg) Sample.

Accession Number	Gene Name	Spec Count
P13596;	Ncam1	344
P68370;Q6P9V9;	Tuba1	116
Q63198;	Cntn1	115
P02770;	Alb	86
P07936;	Gap43	68
P04797;	Gapdh	66
Q5XIF6;	Tuba4a	61
P19332-2;P19332;	Mapt	50
P32736-2;P32736;	Opcml	49
P60711;P63259;	Act	46
P15865;	Hist1h1e	44
P04636;	Mdh2	43
P10111;	Ppia	42
P07340;	Atp1b1	41
Q05695-2;Q05695;	L1cam	39

Accession Number	Gene Name	Spec Count
P17764;	Acat1	24
P00507;	Got2	24
P54290;	Cacna2d1	24
Q05962;	Slc25a4	23
O88989;	Mdh1	21
P62630;	Eef1a1	21
P50137;	Tkt	21
P97685;	Nfasc	21
Q05175;	Basp1	20
Q06647;	Atp5o	20
P16617;	Pgk1	19
P04218;	Cd200	19
P59215;	Gnao1	19
Q63416;	Itih3	19
P11442;	Cltc	19

Supplementary Table 3 Mass Spectrometry Data for Contralateral Cortex (25 mg) Sample, continued.

Accession Number	Gene Name	Spec Count
P15999;	Atp5a1	37
P47942;	Dpysl2	36
P04764;	Eno1	36
P52873;	Pc	36
P63102;	Ywhaz	35
Q9ER34;	Aco2	35
Q62950;	Crmp1	34
P55051;	Fabp7	32
Q62718;	Ntm	30
P10719;	Atp5b	30
P63039;	Hspd1	30
Q09073;	Slc25a5	27
Q6P6R2;	Dld	27
P31399;	Atp5h	26
P31000;	Vim	26
Q9R066-2;Q9R066;	Cxadr	26
P45592;	Cfl1	25
P35213-2;P35213;	Ywhab	25
D3ZBN0;	Hist1h1b	24
P10860;	Glud1	14
Q62813-2;Q62813;	Lsamp	14
P63079;	Gabrb3	14
O88767;	Park7	13
Q9Z0J8;	Negr1	13
Q9JHU0;	Dpysl5	13
Q64428;	Hadha	13
Q920L2;	Sdha	13
P32551;	Uqcrc2	13
Q7M0E3;	Dstn	12
P13086;	Suclg1	12
B2GV06;	Oxct1	12
P16086;	Sptan1	12

Accession Number	Gene Name	Spec Count
Q9ERB4-2;Q9ERB4;	Vcan	18
P61983;	Ywhag	17
P48500;	Tpi1	17
P68255;	Ywhaq	17
P61765-2;P61765;	Stxbp1	17
O35112;	Alcam	17
P85845;	Fscn1	17
P11030;	Dbi	16
P62260;	Ywhae	16
P04642;	Ldha	16
P07335;	Ckb	16
P97603;	Neo1	16
P26772;	Hspe1	15
Q794F9;	Slc3a2	15
P97686-2;P97686;P97686-3;	Nrcam	15
Q62656-2;Q62656;Q62656-3;	Ptprz1	15
P55067;	Ncan	15
O08875;	Dclk1	14
P56574;	Idh2	14
P85108;	Tubb2a	8
O35244;	Prdx6	8
Q99NA5;	Idh3a	8
P23565;	Ina	8
P31422;	Grm3	8
P97527;	Cntn5	8
P46101-2;P46101;	Dpp6	8
Q63716;	Prdx1	7
P11232;	Txn	7
Q66HR2;	Mapre1	7
P97710;	Sirpa	7
P16036;	Slc25a3	7
B3GNI6-2;B3GNI6;B3GNI6-3;	11-Sep	7

Supplementary Table 3 Mass Spectrometry Data for Contralateral Cortex (25 mg) Sample, continued.

Accession Number	Gene Name	Spec Count
P19511;	Atp5f1	11
P10888;	Cox4i1	11
P25113;	Pgam1	11
Q3KRE8;	Tubb2b	11
Q8VHF5;	Cs	11
P06687;	Atp1a3	11
P55053;	Fabp5	10
Q6MG60;	Ddah2	10
P63018;	Hspa8	10
P50399;	Gdi2	10
P35053;	Gpc1	10
P62898;	Cycs	9
P62161;	Calm1	9
P63159;	Hmgb1	9
B0K020;	Cisd1	9
P42123;	Ldhb	9
P69897;	Tubb5	9
Q9EPH2;	Marcksl1	9
P14942;	Gsta4	9
P14408-2;P14408;	Fh	9
Q62952-2;Q62952;	Dpysl3	9
P85834;	Tufm	9
P05708;	Hk1	9
P37377-2;P37377;	Snca	8
P35435;	Atp5c1	8
P17132;Q9JJ54;	Hnrnpc	5
P31044;	Pebp1	5
Q5XI73;	Arhgdia	5
Q1WIM3;	Cadm3	5
Q63610-2;Q63610;	Tpm3	5
P17074;	Rps19	5
P62909;	Rps3	5
P30009;	Marcks	5
P05065;	Aldoa	5

Accession Number	Gene Name	Spec Count
P54311;	Gnb1	7
Q9WVK7;	Hadh	7
P52796;	Efnb1	7
P25286-2;P25286;	Atp6v0a1	7
Q5I0C3;	Mccc1	7
Q9JLT0;	Myh10	7
P14882;	Pcca	7
P29418;	Atp5e	6
B0BNA5;	Cotl1	6
Q9R1Z0-2;Q9R1Z0;	Vdac3	6
Q64361;	Lxn	6
P04905;	Gstm1	6
P10536;Q6NYB7;	Rab1	6
P61107;	Rab14	6
Q812E9-2;Q812E9;	Gpm6a	6
Q505J6;	Slc25a18	6
P13635;	Cp	6
P06686;	Atp1a2	6
O35276;	Nrp2	6
P97536;	Cand1	6
Q1WIM2-2;	Cadm2	6
Q03344;	Atpif1	5
Q00981;	Uchl1	5
P52925;	Hmgb2	5
Q63507;	Rpl14	5
O88775;	Emb	4
P08010;	Gstm2	4
P63025;Q63666;	Vamp	4
Q9QYV1;	Tmeff1	4
P24329;	Tst	4
Q6P9T8;	Tubb4b	4
P12368;	Prkar2a	4
Q9EQS0;	Taldo1	4
P19527;	Nefl	4

Supplementary Table 3 Mass Spectrometry Data for Contralateral Cortex (25 mg) Sample, continued.

Accession Number	Gene Name	Spec Count
D3ZW55;	Itpa	5
P47727;	Cbr1	5
P52759;	Hrsp12	5
P27274;	Cd59	5
O35264;	Pafah1b2	5
P67779;	Phb	5
Q60587;	Hadhb	5
P23965;	Eci1	5
P47819-2;P47819;	Gfap	5
Q63135-2;Q63135;	Cr1l	5
O35814;	Stip1	5
Q99MZ8;	Lasp1	5
Q6P6V0;	Gpi	5
Q68FY0;	Uqcrc1	5
Q01205;	Dlst	5
Q4QRB4;	Tubb3	5
P41562;	Idh1	5
P12007;	Ivd	5
Q4V887;	Slc39a6	5
Q499N5;	Acsf2	5
P50398;	Gdi1	5
Q05140-2;Q05140;	Snap91	5
P15146-2;P15146-3;	Map2	5
P0C2X9;	Aldh4a1	5
Q9R063-2;Q9R063;	Prdx5	4
Q9WUC4;	Atox1	4
P61589;	Rhoa	4
P35434;	Atp5d	4
P11240;	Cox5a	4
Q6MG61;	Clic1	3
P43278;	H1f0	3
P62749;Q5PQN0;	Hpcal/Ncald	3
P40112;	Psmb3	3

Accession Number	Gene Name	Spec Count
Q920Q0;	Palm	4
Q3KR86;	Immt	4
Q6Q629;	Dpp10	4
Q68FR6;	Eef1g	4
P51635;	Akr1a1	4
P23693	Tnni3	4
Q5XI22;	Acat2	4
Q64559-1;Q64559;	Acot7	4
P62944-2;P62944;	Ap2b1	4
Q7TPB1;	Cct4	4
P13264-2;P13264;	Gls	4
P82995;	Hsp90aa1	4
P47858;	Pfkm	4
O88871;	Gabbr2	4
Q9Z2L0;	Vdac1	3
Q63362;	Ndufa5	3
P04906;	Gstp1	3
Q6RUV5;	Rac1	3
P62828;Q8K586;	Ran/Rasl2-9	3
P25886;	Rpl29	3
P26453-2;P26453;	Bsg	3
P61354;	Rpl27	3
P17078;	Rpl35	3
P62836;Q62636;	Rap1	3
Q5BK63;	Ndufa9	3
Q62609-3;Q62609;	Olfm1	3
Q07936-2;Q07936;	Anxa2	3
P05714;Q63941;Q5U316;Q53B90	Rab	3
P07825;	Syp	3
P13668;	Stmn1	2
P10760;	Ahcy	2
Q5XIE6;	Hibch	2
P08081-2;P08081;	Clta	2

Supplementary Table 3 Mass Spectrometry Data for Contralateral Cortex (25 mg) Sample, continued.

Accession Number	Gene Name	Spec Count
O70351;	Hsd17b10	3
P40241;	Cd9	3
P97687;	Entpd1	3
Q8K4Y5;	Lgi1	3
B0BNE5;	Esd	3
Q64057;	Aldh7a1	3
Q66HF8;	Aldh1b1	3
Q66HD0;	Hsp90b1	3
P14740;	Dpp4	3
P84092;	Ap2m1	3
P21533;	Rpl6	3
Q05546-2;Q05546;	Tnr	3
P22791;	Hmgcs2	3
P21396;	Maoa	3
Q68FX0;	Idh3B	3
P28480;	Tcp1	3
Q62889-2;Q62889;	Nlgn3	3
Q8CFG5;	Cacna2d3	3
P22063;	Cntn2	3
Q9EPC6;	Pfn2	2
P62853;	Rps25	2
P62959;	Hint1	2
P63170;	Dynll1	2
Q8CFN2-2;Q8CFN2;	Cdc42	2
P30904;	Mif	2
P62859;	Rps28	2
Q62658;	Fkbp1a	2
B0BNM1;	Apoa1bp	2
P62278;	Rps13	2
P39032;	Rpl36	2
Q6PCU2;	Atp6v1e1	2
P61265;	Stx1b	2
D3ZAF6;	Atp5j2	2
Q923M1-2;Q923M1;	Msra	2
P11598;	Pdia3	2

Accession Number	Gene Name	Spec Count
Q5FVI4;	Cend1	2
P18420;	Psma1	2
P39069;	Ak1	2
P26284;	Pdha1	2
Q5M7U6;	Actr2	2
P17220;	Psma2	2
P13437;	Acaa2	2
P61206;Q5BK71;	Arf	2
P11980-2;P11980;	Pkm	2
Q5RKI0;	Wdr1	2
P49911;	Anp32a	2
Q02253;	Aldh6a1	2
P12711;	Adh5	2
Q9QYU4;	Crym	2
P14668;	Anxa5	2
O88600;	Hspa4	2
Q6PDU1;	Srsf2	2
Q68FU3;	Etfb	2
P97829-2;P97829;	Cd47	2
P11884;	Aldh2	2
P21531;	Rpl3	2
Q6DGG0;	Ppid	2
Q5XIH7;	Phb2	2
P18886;	Cpt2	2
P50554;	Abat	2
Q9WVK3;	Pecr	2
P09117;	Aldoc	2
B4F795;	Slc44a2	2
Q9JMJ4;	Prpf19	2
P61980;	Hnrnpk	2
P13221;	Got1	2
P69060;	Cmas	2
O35077;	Gpd1	2
Q641Z6;Q8R491;	Ehd	2
Q9EQX9;	Ube2n	1

Supplementary Table 3 Mass Spectrometry Data for Contralateral Cortex (25 mg) Sample, continued.

Accession Number	Gene Name	Spec Count
P38652;	Pgm1	2
F1LYQ8;	Farp1	2
Q75Q39;	Tomm70a	2
P97523;	Met	2
Q63424;	Slc15a2	2
Q5FVJ0-2;Q5FVJ0;	Rufy3	2
Q9Z1A5;	Nae1	2
P63004;	Pafah1b1	2
P21588;	Nt5e	2
D4A1J9;	Lrfn5	2
Q3KRE0;	Atad3	2
Q63372-10;Q63372;	Nrxn1	2
Q62915;	Cask	2
P34058;	Hsp90ab1	2
Q66HF1;	Ndufs1	2
P31596-2;P31596;	Slc1a2	2
P31424-2;P31424;	Grm5	2
Q9QUL6;	Nsf	2
P30835;	Pfkl	2
Q9Z1K9;	Adam17	2
P46462;	Vcp	2
P24062;	Igf1r	2
O88278;	Celsr3	2
P11608;	Mt-atp8	1
Q91XV6-2;Q91XV6;	Fxyd6	1
Q91Y55;	Cldn16	1
P35745;	Acyp2	1
P01041;	Cstb	1
P02091;P11517;	Hbb	1
P62845;	Rps15	1
Q63228;	Gmfb	1
P63324;	Rps12	1
Q4KM74;	Sec22b	1
P62282;	Rps11	1
Q6DGF6;	Fam220a	1

Accession Number	Gene Name	Spec Count
D3ZE85;	Frrs1l	1
P85973;	Pnp	1
P29117;	Ppif	1
P14604;	Echs1	1
P13852;	Prnp	1
P83732;	Rpl24	1
P04256;	Hnrnpa1	1
P20788;	Uqcrfs1	1
P47728;	Calb2	1
Q64548-2;Q64548;	Rtn1	1
P62083;	Rps7	1
P70580;	Pgrmc1	1
P62703;	Rps4x	1
P10252;	Cd48	1
P03994;	Hapln1	1
Q6AYG5;	Echdc1	1
Q5XI32;	Capzb	1
P50878;	Rpl4	1
Q9ESI7;	Dcx	1
P97697;	Impa1	1
P63182;	Cbln1	1
P15650;	Acadl	1
Q08406;	Cntfr	1
P21913;	Sdhb	1
P02773-2;P02773;	Afp	1
P16446;	Pitpna	1
D3ZBN0	Hist1h1	1
P47853;	Bgn	1
Q9JLJ3;	Aldh9a1	1
Q5XIT1;	Mapre3	1
P35565;	Canx	1
P63329-2;P63329;	Ppp3ca	1
Q08163;	Cap1	1
Q63569;	Psmc3	1
P11661;	Mtnd5	1

Supplementary Table 3 Mass Spectrometry Data for Contralateral Cortex (25 mg) Sample, continued.

Accession Number	Gene Name	Spec Count
P29314;	Rps9	1
P24368;	Ppib	1
Q9R080-4;Q9R080;	Gpsm1	1
P20272;	Cnr1	1
Q9R1K2-2;Q9R1K2;	Tenm2	1
P12785;	Fasn	1
P21707;	Syt1	1
Q8VHW5;	Cacng8	1
Q9EPH8;	Pabpc1	1
Q63092;	Camkv	1
Q68FS2;	Cops4	1
Q5I0G4;	Gars	1
Q63028-2;Q63028;	Add1	1
P08289;	Alpl	1
P11275;P15791;	Camk2	1
P32215-2;P32215;	Adcyap1r1	1
O89042	Pola1	1
Q07266-2;Q07266;	Dbn1	1
P18418;	Calr	1
P04785;	P4hb	1
Q9Z330-2;Q9Z330	Dnmt1	1
Q5SGE0;	Lrpprc	1

Accession Number	Gene Name	Spec Count
Q5FVM4;	Nono	1
P85968;	Pgd	1
O70277;	Trim3	1
Q5XI51;Q9WV63;	Kif2	1
P70615;	Lmnb1	1
P18484;	Ap2a2	1
P23385-2;P23385;	Grm1	1
P49134;	Itgb1	1
D3ZQG6;	Trim2	1
P48037;	Anxa6	1
O08838;Q68FR2;O08839;	Amph	1
Q63617;	Hyou1	1
Q63270;	Aco1	1
P24942-2;P24942;	Slc1a3	1
P31421;	Grm2	1
P55161;	Nckap1	1
Q9Z0U4-2;Q9Z0U4;	Gabbr1	1
Q07310-10;Q07310;	Nrxn3	1
F1LP90;	Mink1	1
O88902;	Ptpn23	1
P10687;	Plcb1	1

Methods:

Injection Strategy

Postnatal day 3 mouse and rat pups were anesthetized and injected with 4 μL of label in left hemisphere, 3 mm medial and 4 mm caudal of eye (0.2% NHS-Biotin, 5% FastGreen in DMSO).

Immunohistochemistry

Mice pups were anesthetized and perfused intracartically with 5 mLs of ice cold PBS by syringe injection, followed by 5 mLs of ice cold 4% PFA. Collected brains were post-fixed in 4% PFA overnight at 4℃. Brains were embedded in 6% agarose for vibratome sectioning at approximately 50-60 μm slices. Medial coronal sections, containing visible corpus callosum were blocked with 5% normal donkey serum (NDS) and 0.5% Triton in PBS for 40 minutes at room temperature. Primary antibodies were added at the recommended concentration by the manufacturer (1:600 GαBiotin and sequentially candidate proteins) and incubated for two days at 4℃. Sections were washed 3X with 0.5% Triton in PBS. AlexaFluoro conjugated secondary antibodies were added and incubated overnight at 4℃. Sectioned were washed 3X with 0.5% Triton in PBS, with the last wash including Hoechst 33342. Sections were imaged at 20, 40 and 60X magnification on Leica C2 Confocal Microscope. Images were visualized and processed in ImageJ.

Dissection Strategy

Mice were anesthetized and decapitated following IACUC guidelines and regulations. The brain was carefully retracted from surrounding skull but dissecting along the sagittal suture to remove parietal and frontal bones. The brain was mounted on a petri dish over a plate of dry ice to divide the brain along midline into two hemispheres. The left (injected,

ispilateral) hemisphere was placed on dry ice during the dissection of the right (contralateral) hemisphere. 1 mm coronal sections were made to visualize and dissect the entirety of the corpus callosum, from rostral to caudal. The cortical tissue was collected in a separate microfuge tube, similarly the cerebellum was collected in a separate microfuge tube. All samples were kept on dry ice. This dissection process was repeated with the ipsilateral hemisphere. Tissue samples were homogenized with RIPA and a protease inhibitor cocktail and kept at -80℃ until further processing.

Western Blot

The protein concentration of homogenized samples was determined via Bradford assay. SDS-PAGE gel was run for all dissected samples with BioRad precast 18 well gels, with 20 μg of protein in each well and rainbow molecular weight ladder. SDS-PAGE was run at 120 V for 45 minutes and transferred onto BioRad nitrocellulose membrane by the Trans-Blot Turbo Transfer System. Nitrocellulose membrane was incubated in Ponceau for 3 minutes, washed with diH_2O and imaged. Nitrocellulose membrane was blocked with 5% non-fat milk in 0.05% Tween 20 in TBS for 40 minutes at room temperature. Membrane was washed in 0.05% Tween 20 TBS 3X and incubated with primary antibodies at manufacturers recommended concentrations, overnight at 4℃. Membrane was washed 3X and incubated for 2 hours at room temperature with HRP conjugated secondary antibodies. Membrane was washed 3X and imaging media was added for 2 minutes. Film was exposed in the dark room by HRP signal, fixed and imaged.

Immunoprecipitation

Homogenized and quantified protein samples were immunoprecipitated by high capacity streptavidin conjugated agarose beads. Beads were washed with PBS 3X and centrifuged at 1500 RPM. 20 μL of homogenized sample was added to the beads and incubated

overnight at 4℃. Beads were washed 3X with PBS and biotinylated proteins were eluted with sample buffer (SDS and β-mercaptoethanol) by boiling the sample to disrupt streptavidin-biotin affinity.

Mass Spectrometry Sample Preparation

Protein was precipitated from pooled samples via 5 mg aliquots of protein. 200 μL of sample was added to individual tubes to maximize precipitation efficiency; followed by 600 μL of methanol. Sample was vortexed and 200 μL of chloroform was added, followed by 500 μL of water. Sample was centrifuged at 14,000 RPM for 5 minutes at room temperature. Liquid was decanted and 600 μL of methanol was added by a secondary centrifugation with the same parameters. Sample was decanted and 400 μL of methanol was added. To resuspend the pellet was sonicated and combined to achieve the initial 5 mg protein sample. Sample was centrifuged with the same parameters, decanted and frozen at -80℃ until the digestion stage.

Frozen pellet was resuspended in 8 M urea in 100 mM Tris to achieve a pH of 8. 5 mM of TCEP was added and incubated at 37℃ for 30 minutes. 10 mM of IAA was added and incubated at room temperature for 30 minutes. The sample was diluted to a final 2 M urea concentration and a 1:25 concentration of trypsin was incubated overnight at 37℃. 10% TFA was added to reach a sample concentration of 0.1% and centrifuged at room temperature at 14,000 RPM for 15 minutes. The supernatant was transferred and saved; the pellet was resuspended by sonication in 0.1% TFA and centrifuged for 15 minutes at 14,000 RPM. The supernatants were combined and proceeded to the desalting protocol.

SepPak solid-phase extraction cartridges were used to desalt peptide sample. Using a vacuum seal, 3 mL of 100% acetonitrile (ACN) was added, followed by 3 mL of 50% ACN and 0.5% acetic acid (AA). 3 mL of 0.1% TFA was added, followed by the loading of our

sample into the column. Sample was washed with 3 mL 0.1% TFA and 250 μL of 0.5% AA. Into a clean collection tube, the sample was eluted with 1 mL of 80% ACN and 0.5% AA. The elution was dried in spin vacuum and finally resuspended in PBS.

The resuspended peptide samples were added to Neutravidin beads that had been washed 3X with PBS. The sample in neutravidin beads were washed 3X with water, 3X with 5% ACN in PBS and 3X with diH_2O. The remaining supernatant was removed with syringe and 200 μL of the elution buffer was added (0.2% TFA, 0.1% Formic Acid, 80% ACN). The beads were incubated at room temperature for 5 minutes. The supernatant was collected and 200 μL of elution buffer was added to the beads and incubated at 70℃ for 5 minutes. The supernatants were combined, dried and sent for mass spectrometry evaluation.

The results from mass spectrometry were evaluated and compared to sequence databases: UniProt, PANTHER and BioVenn.

REFERENCES

Alfonso, J., Fernandez, M., Cooper, B., Flugge, G., Frasch A. The stress-regulated protein M6a is a key modulator for neurite outgrowth and filopodium/spine formation. *Proc. Natl. Acad. Sci.* (2005)

Anderson, G., Galfin, T., Xu, W., Aoto, J., Malenka, R., and Südhof, T. Candidate Autism Gene Screen Identifies Critical Role for the Cell-Adhesion Molecule CASPR2 in Dendritic Arborization and Spine Development. *PNAS* (2012).

Arlotta, P., Molyneaux, B., Chen, J., Inoue, J., Kominami, R., Macklis, J. Neuronal Subtype-Specific Genes that Control Corticospinal Motor Neuron Development In Vivo. *Neuron* (2005).

Becker, S., Mayor, R., Kashet, J. Cadherin-11 Mediates Contact Inhibition of Locomotion during *Xenopus* Neural Crest Cell Migration. *PLOS* (2013).

Cagnetta, R., Frese, C., Shigeoka, T., Krijgsveld, J., Holt, C. Rapid Cue-Specific Remodeling of the Nascent Axonal Proteome. *Neuron* (2018).

Campbell, D., Holt, C. Chemotropic Responses of Retinal Growth Cones Mediated by Rapid Local Protein Synthesis and Degradation. *Neuron* (2001).

Chamberlin, N. L., Du, B., de Lacalle, S. & Saper, C. B. Recombinant adeno-associated virus vector: use for transgene expression and anterograde tract tracing in the CNS. *Brain Res* (1998).

Comer, J.D., Alvarez, S., Butler, S.J. Kaltzschmidt, J. Commissural axon guidance in the developing spinal cord: from Cajal to the present day. *Neural Dev* 14, 9 (2019)

Demyanenko GP, Mohan V, Zhang X[1], Brennaman, L., Dharbal, K., Tran, T., Manis, P., Maness, P., Neural cell adhesion molecule NrCAM regulates Semaphorin 3F-induced dendritic spine remodeling. *J Neurosci*. (2014).

Faulkner, R., Low, L., Liu, X., Coble, J., Jones, E., Cheng, H. Dorsal Turning of Motor Corticospinal Axons at the Pyramidal Decussation Requires Plexin Signaling. *Neural Dev* (2008).

Han, S., Li, J., Ting, A. Proximity Labeling: Spatially Resolved Proteomic Mapping for Neurobiology. *Current Opinion in Neurobiology* (2018).

Kanijo, S., Ishii, Y., Horigane, S., Suzuki, K., Ohkura, M., Nakai, J., Fujii, H., Takemoto-Kimura, S., Bito, H. A Critical Neurodevelopmental Role for L-Type Voltage-Gated Calcium Channels in Neurite Extension and Radial Migration. *The Journal of Neuroscience* (2018).

Kristensson K, Olsson Y. Retrograde axonal transport of protein. *Brain Res* (1971)

Kullander, K., Mather, N., Diella, F., Dottori, M., Boyd, A., Klein, R. Kinase-Dependent and Kinase-Independent Functions of EphA4 Receptors in Major Axon Tract Formation In Vivo. *Neuron* (2001).

Lerner, T. N., Ye, L. & Deisseroth, K. Communication in neural circuits: tools, opportunities, and challenges. *Cell* (2016)

Li, H., Leung, T., Hoffman, S., Balsamo, J., Lilien, J. Coordinate Regulation of Cadherin and Integrin Function by the Chondrotin Sulfate Proteoglycan Neurocan. *J Cell Biol* (2000).

Milev P, Maurel P, Chiba A. Differential regulation of expression of hyaluronan-binding proteoglycans in developing brain: aggrecan, versican, neurocan, and brevican. *Biochem Biophys Res Commun*. (1998)

Milev, P., Maurel, P., Häring, M., Margolis, R, Margolis, R. TAG-1/Axonin-1 is a High-Affinity Ligand of Neurocan, Phosphacan/Protein Tyrosine Phosphatase-ζ/β. *Journal of Biological Chemistry* (1996).

Nakamura F, Kalb RG, Strittmatter SM. Molecular basis of semaphorin-mediated axon guidance. *J Neurobiol*. (2000)

Nudell, V., (2019). *CLARITY Whole-Brain Imaging.* Unpublished Raw Data.

Poulopoulos, A., Murphy, A.J., Ozkan, A.. Subcellular transcriptomes and proteomes of developing axon projections in the cerebral cortex. *Nature* (2019).

Retzler, C., Göhring, W., Rauch, U. Analysis of Neurocan Structures Interacting with the Neural Cell Adhesion Molecule (Ncam). *Journal of Biological Chemistry* (1996).

Robichaux MA, Chenaux G, Ho HY. EphB1 and EphB2 intracellular domains regulate the formation of the corpus callosum and anterior commissure. *Dev Neurobiol*. (2016)

Sakaguchi, R., Leiwe, M. N. & Imai, T. Bright multicolor labeling of neuronal circuits with fluorescent proteins and chemical tags. *Elife* (2018).

Saleeba, C., Dempsey, B., Le, S., Goodchild, A., and McMullan, S. A Student's Guide to Neural Circuit Tracing. *Frontiers in Neuroscience* (2019).

Schiapparelli, L., McClatchy, D., Liu, H., Sharma, P., Yates, J., and Cline, H. Direct Detection of Biotinylated Proteins by Mass Spectrometry. *Journal of Proteome Research* (2014).

Schiapparelli, L., Shah, S., Ma, Y., McClatchy, D., Sharma, P., Li, J., Yates, J., Goldberg, J., Cline, H. The Retinal Ganglion Cell Transportome Identifies Proteins Transported to Axons and Presynaptic Compartments in the Visual System *in vivo*. *Science Direct* (2019).

Sharma, P., (2019). *NHS-Biotin Injections in Developing Rodent Brain.* Unpublished Raw Data.

Stoll, G., Jander, S., Myers, R. Degeneration and Regeneration of the Peripheral Nervous System: From Augustus Waller's Observations to Neuroinflammation. *Journal of the Peripheral Nervous System*, vol. 7, no. 1, (2002)

Ughrin, Y,, Chen, Z., Levine, J. Multiple Regions of the NG2 Proteoglycan Inhibit Neurite Growth and Induce Growth Cone Collapse. *Journal of Neuroscience* (1996).

Yamaguchi, Y., Heparan Sulfate Proteoglycans in the Nervous System: Their Diverse Roles in Neurogenesis, Axon Guidance and Synaptogenesis. *Cell and Dev. Bio.* (2001).